

8478
NACA TN 2010

TECH LIBRARY KAFB, NM
0065269

NATIONAL ADVISORY COMMITTEE FOR AERONAUTICS

TECHNICAL NOTE 2010

EFFECT OF HORIZONTAL TAIL ON LOW-SPEED STATIC LATERAL
STABILITY CHARACTERISTICS OF A MODEL HAVING
45° SWEEPBACK WING AND TAIL SURFACES

By Jack D. Brewer and Jacob H. Lichtenstein

Langley Aeronautical Laboratory
Langley Air Force Base, Va.



Washington
January 1950

AFMDC
TECHNICAL LIBRARY
AFL 2811



NATIONAL ADVISORY COMMITTEE FOR AERONAUTICS

TECHNICAL NOTE 2010

EFFECT OF HORIZONTAL TAIL ON LOW-SPEED STATIC LATERAL

STABILITY CHARACTERISTICS OF A MODEL HAVING

45° SWEEPBACK WING AND TAIL SURFACES

By Jack D. Brewer and Jacob H. Lichtenstein

SUMMARY

An investigation has been conducted in the Langley stability tunnel to determine the effects of changes in horizontal-tail size and location on the static lateral stability characteristics of a complete model with wing and tail surfaces having the quarter-chord line swept back 45°.

Available procedures, based on analyses of unswept-tail configurations, for predicting the effect of the horizontal tail on directional stability, were found to be unreliable when applied to swept-tail configurations.

When the horizontal tail was located at the base of the vertical tail, displacement of the horizontal tail rearward increased the favorable contribution of the horizontal tail to directional stability at low angles of attack; at high angles of attack, the contribution of the horizontal tail was unfavorable regardless of the horizontal location. When the horizontal tail was located near the top of the vertical tail, the contribution of the horizontal tail was highly favorable at low angles of attack; at high angles of attack, the largest favorable effect was obtained with the horizontal tail in a forward location.

The trends obtained with the wing on were similar to those obtained with the wing off, but a large decrease occurred in the favorable effect obtained at large angles of attack with the horizontal tail in the upper positions; a probable explanation was the detrimental effect of the wing wake arising from flow separation over the wing.

INTRODUCTION

Recent advances in the understanding of the principles of high-speed flight have led to significant changes in the design of the major

component parts of airplanes. In many instances, consideration is given to configurations which are beyond the range covered by available design information regarding stability characteristics. The effects of changes in wing design on stability characteristics have been extensively investigated. In order to provide information on the influence of other parts of the complete airplane, an investigation of a model having various interchangeable component parts is being conducted in the Langley stability tunnel. As part of this investigation, the effect of changes in the size and location of a swept horizontal tail on the static-lateral-stability derivatives was determined.

The effect of the horizontal tail has been rather extensively investigated previously for airplanes having unswept wing and tail surfaces. As a result of an analysis of test results of several models, some simple rules for estimating the contribution of complete tail configuration have been proposed in reference 1. Results showing the effect of horizontal-tail size and location on the vertical-tail contribution are presented in reference 2.

The present investigation was made, therefore, to check the validity of the earlier analyses when applied to configurations incorporating swept wing and tail surfaces.

SYMBOLS

The data presented herein are in the form of standard NACA coefficients of forces and moments which are referred to the stability system of axes with the origin at the projection on the plane of symmetry of the calculated aerodynamic center of the wing. The positive directions of the forces, moments, and angular displacements are shown in figure 1. The coefficients and symbols are defined as follows:

C_L	lift coefficient (L/qS)
C_X	longitudinal-force coefficient (X/qS_W); $C_X = -C_D$ at $\psi = 0$
C_Y	lateral-force coefficient (Y/qS_W)
C_l	rolling-moment coefficient ($L'/qS_W b_W$)
C_m	pitching-moment coefficient ($M/qS_W \bar{c}_W$)
C_n	yawing-moment coefficient ($N/qS_W b_W$)

L	lift
X	longitudinal force; $X = -D$ at $\psi = 0$
Y	lateral force
L'	rolling moment
M	pitching moment
N	yawing moment
q	dynamic pressure
S	area
b	span, measured perpendicular to fuselage center line
c	chord, measured parallel to fuselage center line
\bar{c}	mean aerodynamic chord
\bar{x}	chordwise distance from leading edge of wing root chord to quarter chord of wing mean aerodynamic chord
d	chordwise distance from leading edge of vertical-tail local chord to $\bar{c}_H/4$
\bar{d}	chordwise distance from $\bar{c}_V/4$ to $\bar{c}_H/4$
l	tail length, distance from model mounting point to $\bar{c}_V/4$
A	aspect ratio (b^2/S)
A_e	effective aspect ratio, corresponding to theoretical lift-curve slope
λ	taper ratio
α	angle of attack
ψ	angle of yaw

$$C_{L\alpha} = \frac{\partial C_L}{\partial \alpha}$$

$$C_{m\alpha} = \frac{\partial C_m}{\partial \alpha}$$

$$C_{Y\psi} = \frac{\partial C_Y}{\partial \psi}$$

$$C_{n\psi} = \frac{\partial C_n}{\partial \psi}$$

$$C_{z\psi} = \frac{\partial C_z}{\partial \psi}$$

$$\left. \begin{array}{l} (\Delta C_{Y\psi})_H, (\Delta C_{n\psi})_H, \\ (\Delta C_{z\psi})_H \end{array} \right\}$$

increment resulting from addition of horizontal tail

(for example, $(\Delta C_{Y\psi})_H = (C_{Y\psi})_{\text{Model with H}}$

$- (C_{Y\psi})_{\text{Model without H}}$)

$$(\Delta C_{n\psi})_{V+H}$$

increment resulting from combination of vertical tail

and horizontal tail $((C_{n\psi})_{\text{Model with tail}}$

$- (C_{n\psi})_{\text{Model without tail}}$)

K_{S_H} horizontal-tail-area correction factor

$$\left(\frac{\left[\frac{(A_{\theta_V})_{H \text{ on}}}{(A_{\theta_V})_{H \text{ off}}} \right]_{S_H/S_V} - 1}{\left[\frac{(A_{\theta_V})_{H \text{ on}}}{(A_{\theta_V})_{H \text{ off}}} \right]_{\frac{S_H}{S_V}=1.33} - 1} \right)$$

Subscripts:

- W wing
- F fuselage
- V vertical tail
- H horizontal tail
- r root
- t tip

APPARATUS, MODELS, AND TESTS

The general research model used for the present investigation was designed to permit tests of the wing alone, fuselage alone, or the fuselage in combination with any of several tail configurations - with or without the wing. A sketch of the complete model with one particular tail configuration is shown in figure 2. A list of the pertinent geometric characteristics of various component parts is given in table I. All parts were constructed of mahogany.

The fuselage was a body of revolution having a circular-arc profile (fineness ratio 6.67). The wing and horizontal-tail surfaces had an aspect ratio of 4.0, a taper ratio of 0.6, and an NACA 65A008 profile (in sections parallel to the plane of symmetry); the quarter-chord line was swept back 45° . The vertical tail was of the same sweep, taper ratio, and section but had an aspect ratio of 1.0. Ordinates for the NACA 65A008 airfoil section are given in table II.

For the present investigation, horizontal tails of three different areas were used. These tails are designated as H_1 , H_2 , and H_3 (in the order of increasing area) in table I and figure 3. Horizontal tails H_1 and H_3 were tested in only one location (the low middle location). Horizontal tail H_2 was tested at three horizontal locations for each of three vertical positions, as illustrated in figure 4. In referring to the horizontal-tail configurations, the letters L, C, and U indicate the vertical position as being lower, center, or upper, respectively; and the letters F, M, and R indicate the horizontal location as being forward, middle, or rearward, respectively. (A horizontal tail designated $(H_2)_{CF}$, therefore, represents the horizontal tail of intermediate area mounted in the central vertical position and in the forward horizontal location.) Most of the fuselage-tail combinations were tested with and without the wing mounted on the model. A complete list of the configurations investigated is presented in table III.

The model was rigidly mounted on a single strut at the point shown in figure 2. Forces and moments were measured by means of a conventional six-component balance system.

A photograph of a complete configuration is presented as figure 5.

In order to obtain the lift-curve slope of the isolated vertical tail, the tail was mounted on a small rod above the strut. The mounting arrangement for this configuration is shown in figure 6.

Tests were made at a dynamic pressure of 24.9 pounds per square foot, which corresponds to a Mach number of 0.13 and to a Reynolds number of 0.71×10^6 , based on the wing mean aerodynamic chord. The angle of attack was varied from about -4° to 30° for angles of yaw of 0° and $\pm 5^\circ$. The horizontal-tail incidence was kept at 0° for all tests.

CORRECTIONS

The angle of attack, longitudinal-force coefficient, pitching-moment coefficient, and rolling-moment coefficient have been corrected for the effects of jet boundaries. The data are not corrected for blocking, turbulence, or support-strut interference.

RESULTS AND DISCUSSION

Presentation of Data

Results of the investigation are given in three parts. The first part, consisting of figures 7 to 10, presents the longitudinal and lateral stability characteristics of certain basic configurations, including the fuselage alone, the wing alone, the wing-fuselage combination, and one complete configuration. The second part (figs. 11 and 12) shows the effects on the lateral-stability derivatives of variations in the area of the horizontal tail (when located in the LM position). The effects on the lateral-stability derivatives of variations in the vertical and horizontal location of the intermediate-size horizontal tail (H_2) are presented in the third part (figs. 13 to 18).

The model configurations are identified in the figures by the system of abbreviations explained in table III.

Characteristics of Some Basic Configurations

The pitching-moment results for the wing alone, presented in figure 7, show the aerodynamic center to be located at $0.25\bar{c}_w$ which is in good agreement with the theoretical value given in reference 3 ($0.26\bar{c}_w$). The isolated fuselage is shown to give the expected unstable value of C_{m_α} , but the wing-fuselage combination has about the same value of C_{m_α} (at small angles) as the wing alone. The stability obtained with the wing-fuselage combination is in qualitative agreement with results of an unpublished analysis made by Schlichting and is attributed to the loss in load over the wing near the wing-fuselage juncture and to the alteration in fuselage loading effected by the upwash in front of the wing. (See, for example, reference 4.)

In interpreting data of configurations including a wing, consideration must be given to the angle-of-attack range over which the flow does not separate from the wing. As pointed out in reference 5, an indication of the limit of this range can be obtained by locating the initial break in the plot of $C_D - \frac{C_L^2}{\pi A_W}$ against angle of attack.

Figure 8 presents a plot of this increment for the wing tested; the curve is shown to break at an angle of attack of approximately 7° . Corresponding breaks for the wing-alone tests are shown in the pitching-moment curves and lift-coefficient curves in figure 7 and in the plots of C_{Y_ψ} and C_{Z_ψ} (fig. 9). A change in the wing-wake characteristics would also be expected at this angle, and the resultant effects of the vertical and horizontal tails would probably be somewhat erratic.

Results for a complete configuration show that negative values of C_{n_ψ} are provided up to an angle of attack of 19° . (See fig. 9.) The tendency to become unstable at higher angles is attributed both to the basic instability of the wing at those angles and to the decreased effectiveness of the vertical tail due to the wing and fuselage wake. An increase in Reynolds number or use of a device that would delay separation from the wing probably would improve the directional stability of the complete model at high angles. The positive increase for the complete model in C_{Z_ψ} at $\alpha = 0^\circ$ is provided mainly by the vertical tail; as the angle of attack is increased, the moment arm decreases, so that the increment and consequently the slope of C_{Z_ψ} against α decreases.

The lift-curve slopes of the wing and of the isolated vertical tail are compared with theory in figure 10. Tests were made on the vertical tail alone (see fig. 6) to eliminate any interference effects produced by the fuselage or horizontal tail. The experimental lift-curve slope of the vertical tail (0.027) is shown to be about 13 percent higher than that predicted by the theory. Other tests (for example, reference 6) have shown that C_{L_α} for sweptback surfaces of low aspect ratio is generally underestimated by the theory. The experimentally determined value of C_{L_α} for the wing (0.054) is in fairly close agreement with the theoretical value (0.052).

Effect of Horizontal-Tail Area

The effect of a change in area of the horizontal tail (H_{TM}) with the wing off is shown in figure 11. With the vertical tail off, the

effect of the horizontal tail on the static-lateral-stability parameters generally was negligible except at very high angles of attack where increasing area had a beneficial effect on the directional stability. With the vertical tail on, an increase in horizontal-tail area had a favorable effect on $C_{n\psi}$ at small angles of attack. At large angles of attack an increase in area generally had a detrimental effect, probably because of flow separation at the juncture of the horizontal tail.

The increments in $C_{n\psi}$ effected by the horizontal tail and by the combination of the vertical tail and the horizontal tail are presented in figure 12(a) for angles of attack of 0° , 10° , and 20° . In order to make these data comparable with data on unswept surfaces the increment in $C_{n\psi}$ was converted to a lift-curve slope by means of the relation

$$\left(C_{L\alpha}\right)_{V,H \text{ on}} = -\left(\Delta C_{n\psi}\right)_{V+H} \frac{b_W S_W}{l S_V}$$

and the corresponding effective aspect ratio of the vertical tail obtained from figure 10. The directional-stability parameter $C_{n\psi}$ rather than $C_{Y\psi}$, was used since it is considered the more important, as well as the more reliable, parameter. It appears probable that the presence of the horizontal tail and fuselage changed the flow characteristics in the region of the vertical tail, thereby altering the effective tail length somewhat; consequently, the lift-curve slope determined from the increment in $C_{n\psi}$ could be expected to be different from one determined by the increment in $C_{Y\psi}$. Some inconsistency between increments of $C_{n\psi}$ and increments of $C_{Y\psi}$ results from the nature of the precision of measurement. An increment determined by the difference of two quantities, each of which is large relative to the increment in question usually cannot be evaluated with high accuracy. In this respect, an analysis based on $C_{n\psi}$ is considered to be more reliable than an analysis based on $C_{Y\psi}$, since the model fuselage reduces the values of $C_{n\psi}$ but increases the values of $C_{Y\psi}$. The effect of horizontal-tail area on the effective aspect ratio of the vertical tail for $\alpha = 0^\circ$ is given in figure 12(b). The lower curve $\left(A_{eV}\right)_{H \text{ on}} / \left(A_{eV}\right)_{H \text{ off}}$ shows the effect of the horizontal tail, including the contribution of the tail itself and its end-plate effect. A similar ratio is presented in figure 17 of reference 2 for unswept horizontal-tail surfaces. Although

the results of reference 2 appear to agree well with the swept-tail results, they may not actually be comparable because the curves of reference 2 are representative only of a configuration having the root chords of the vertical and horizontal tails equal, whereas the present results represent configurations in which the root chord of the horizontal tail was considerably shorter than that of the vertical tail. The effect of a change in horizontal-tail chord on the end-plate effect is not known. The middle curve $\left(\left(A_{eV} \right)_H \text{ on } \left(A_{eV} \right)_V \text{ isolated} \right)$ shows the effects contributed by the horizontal tail and also those contributed by the fuselage. Reference 1 indicated that a usual value for this ratio was 1.55 for unswept tail surfaces. This value is seen to be greatly in excess of the present values obtained with swept surfaces. The upper curve $\left(\left(A_{eV} \right)_H \text{ on } A_V \right)$ accounts for (in addition to the effects of the horizontal tail and fuselage) the limitations of the theory for predicting $\left(C_{L\alpha} \right)_V$. The difference between the upper and middle curves indicates the error that would be obtained if the theoretical $C_{L\alpha}$ were used for this aspect ratio. It is expected that this error will decrease as the aspect ratio of the surface increases.

It should be pointed out that a change in horizontal-tail incidence would be expected to affect the horizontal-tail contribution; however, the effect of change in tail incidence was not investigated in the present tests - the tail having an incidence of 0° on all configurations.

Effect of Horizontal-Tail Displacement

The effect on the lateral-stability derivatives of longitudinal displacement of the horizontal tail for each of three vertical positions is shown in figure 13 for the model with the wing off and in figure 14 for the model with the wing on. The lateral stability characteristics for the model with horizontal tail removed are presented in figure 15 in order that the incremental contribution of the horizontal tail may be determined. The effects of variations in the horizontal-tail location are shown most clearly by means of the plots presented in figure 16 of the increments $\left(\Delta C_{Y\psi} \right)_H$, $\left(\Delta C_{N\psi} \right)_H$, and $\left(\Delta C_{l\psi} \right)_H$ resulting from the addition of the horizontal tail. The abscissa scale indicates the longitudinal location of the aerodynamic center of the horizontal tail; the vertical location of the abscissa scale shows the vertical level of the horizontal tail.

Because the magnitudes of the increments considered generally are small, complete consistency of the results cannot be expected; however, the trends resulting from systematic variations in the tail configuration

are considered to be reliable. Of the increments $(\Delta C_{Y\psi})_H$ and $(\Delta C_{n\psi})_H$ the latter is believed to provide the more reliable indication of the influence of the horizontal tail on vertical-tail effectiveness, as was pointed out in the previous section.

Wing off.— With the wing off, rearward movement of the tail (in the lower position) resulted in an increase in directional stability and $C_{Y\psi}$ at low angles of attack. (See figs. 13(a) and 16.) This result is in qualitative agreement with results obtained in reference 2 for unswept horizontal tails. At higher angles, the directional stability approached zero regardless of the longitudinal location of the tail. The beneficial result of the rearward movement is attributed partly to an increase in the end-plate contribution of the horizontal tail, for when the horizontal tail is mounted in a region where the fuselage is rather thick, it is unable to produce much additional end-plate effect to that already supplied by the fuselage. In the more rearward positions, where the fuselage is thin, the end-plate effect of the horizontal tail is more apparent. The change in $C_{Y\psi}$ and $C_{n\psi}$ with an increase in angle of attack is also not unexpected; as the angle of attack increases, the effective sweep of the vertical tail increases and, since the lift-curve slope of a lifting surface usually decreases with an increase in sweep, a loss in $C_{Y\psi}$ (and $C_{n\psi}$) occurs. The loss becomes greater at the higher angles where the fuselage boundary layer envelops the lower portion of the vertical tail; shielding by the horizontal tail probably causes a further decrease in the vertical-tail effectiveness.

The theory presented in reference 2 indicates that little or no end-plate effect should be expected from the horizontal tail when it is in the central vertical position. The present results show that the horizontal tail, when mounted in this position, had even a slightly adverse effect in most instances; that is, the combination of the vertical tail and the horizontal tail produced smaller increments in the parameters than the vertical tail alone. (See fig. 16.) There was almost no change in vertical-tail effectiveness with increasing angle of attack (until large angles) probably because the downwash of the horizontal tail itself tended to counteract the unfavorable effect of the increased sweepback. (See fig. 13(b).) At high angles of attack, a loss occurs in $C_{Y\psi}$ and $C_{n\psi}$, as it did for the lower positions, presumably because of adverse effects of the fuselage boundary layer over the lower portion of the vertical tail and shielding by the horizontal tail.

When the horizontal tail is mounted in the upper positions, the full end-plate effect of the horizontal tail is realized in addition to the effect supplied by the fuselage. The most favorable increments in $C_{Y\psi}$

and $C_{n\psi}$, therefore, are obtained for the horizontal tail in these positions (fig. 16). The variation of the increments in $C_{Y\psi}$ and $C_{n\psi}$ with angle of attack was found to be slightly favorable for the horizontal tail in the upper positions; at large angles, the effectiveness of the vertical tail did decrease, but less rapidly than when the horizontal tail was mounted in either of the lower positions. (See fig. 13(c).) At zero angle of attack, a change in longitudinal location (for the upper vertical position) had little effect on the increments; but at higher angles the most favorable longitudinal position — from the standpoint of directional stability — was found to be the one farthest forward, for, with the horizontal tail in the rearward location, presumably only a portion of its downwash can counteract the effects of the increased effective sweep of the vertical tail (brought about by the increase in angle of attack). In the forward location, however, the portion of the vertical tail affected by the downwash should be greater and more favorable values of the $C_{Y\psi}$ and $C_{n\psi}$ result; the horizontal tail probably also supplies the greatest end-plate effect in this location, since it covers the portion of the vertical tail where the pressure difference between the two surfaces (and consequently the tip flow) is greatest.

Wing on.— The trends obtained with the wing on (figs. 14 and 16) are generally the same as those obtained with the wing off, but the advantages of the upper positions at high angles of attack appear to be greatly diminished, probably because of the wake behind the wing which is partly stalled at those angles. The favorable results obtained with the wing off probably could be more nearly obtained if a device (for example, slats) was installed on the wing to prevent flow separation.

General.— The results would appear to indicate that the optimum location for the tail was farther rearward (at low angles) for the lower positions and farther forward (at high angles) for the upper positions than the extreme positions investigated herein. Therefore, brief tests (not presented) were made with the horizontal tail mounted in the lower position and in a location farther back than the rearmost location presented (so that $\frac{d}{c_V} = 0.4$). The results showed a decrease in tail effectiveness at $\alpha = 0^\circ$, the values of the increments being approximately equal to those obtained for $\frac{d}{c_V} = 0$ (fig. 16). No additional tests were made in the upper positions, but it is doubtful that much additional effectiveness could be attained at $\alpha = 20^\circ$ by moving the horizontal tail farther forward because of the possible loss of end-plate effectiveness.

As the horizontal tail is moved up (at low angles of attack) the increment in $C_{L\psi}$ tends to change in a positive direction. This may be due, in part, to an upward shift in the center of pressure of the vertical tail. It is probable, however, that a more important effect results from the antisymmetrical load induced on the horizontal tail by the tip vortices associated with the load carried by the vertical tail. With the horizontal tail in the lower position, the tip vortex at the base of the vertical tail would be expected to have the predominant effect and would tend to produce a negative increment in $C_{L\psi}$. The opposite effect (positive increment in $C_{L\psi}$) would be expected when the tail is in the upper position.

The changes in vertical-tail effective aspect ratio (determined as described previously from the increment $(\Delta C_{n\psi})_H$ given in fig. 16) are shown in figure 17. The variation of $(A_{eV})_H \text{ on} / (A_{eV})_H \text{ off}$ with horizontal displacement is substantially greater than that obtained with unswept-tail surfaces (reference 2). The values of $(A_{eV})_H \text{ on} / (A_{eV})_V \text{ isolated}$, which include the effect of fuselage interference, are seen to be generally less than the value of 1.55 suggested for unswept tail surfaces in reference 1.

In order to make these results comparable with unswept-tail results, the more general curves of figure 18 were determined (by interpolation and, in some cases, extrapolation of the curves of fig. 17). The theoretical curve predicted by analyses of unswept-tail results (reference 2) is included and shows consistently larger values for the ratio, although the variation with vertical position of the tail was generally similar. The curves presented are for an angle of attack of 0° only, and it has been previously noted that an increase in angle of attack generally decreases the directional stability in the lower and center positions and consequently reduces the ratio. In the upper positions, an increase in α results in an increase in the value of the ratio to a value substantially greater than that predicted by theory (for example, in the UF position the value of $(A_{eV})_H \text{ on} / (A_{eV})_H \text{ off}$ at $\alpha = 20^\circ$ was 2.1). These results are further indications of the unreliability of present methods (based on unswept-tail results at an angle of attack of 0°) in predicting the effect of swept-tail surfaces on the lateral-stability derivatives.

Application to Design

Although the present investigation was conducted with specific wing and tail plan forms and for a specific fuselage, the results should be suitable for making estimates of the horizontal-tail

contribution to the directional stability of any airplane having approximately the configuration of the model tested. In the usual case, the tail contribution to directional stability is expressed as

$$\Delta C_{n\psi} = -\left(C_{L\alpha}\right)_V \frac{S_V l}{S_W b_W}$$

where $\frac{S_V l}{S_W b_W}$ is frequently referred to as the tail-volume coefficient,

and the vertical-tail lift-curve slope $\left(C_{L\alpha}\right)_V$ may be obtained from

theory (such as reference 3) when the sweep angle, the taper ratio, and the effective aspect ratio A_{eV} are known. The problem, therefore, is

to estimate the effective aspect ratio A_{eV} of the vertical tail when in the presence of the fuselage and horizontal tail. A possible expression for the effective aspect ratio of the vertical tail is as follows:

$$A_{eV} = (A_{eV})_{H \text{ off}} + K_{SH} \left[(A_{eV})_{H \text{ on}} - (A_{eV})_{H \text{ off}} \right]$$

which also can be written in the form

$$A_{eV} = (A_{eV})_{H \text{ off}} \left\{ 1 + K_{SH} \left[\frac{(A_{eV})_{H \text{ on}}}{(A_{eV})_{H \text{ off}}} - 1 \right] \right\} \quad (1)$$

The effective aspect ratio of the vertical tail in the presence of the fuselage $(A_{eV})_{H \text{ off}}$ was found, for the configuration investigated, to

be about 1.17 times the effective aspect ratio of the isolated vertical tail. This factor, however, would be expected to depend on the shape and size of the fuselage, particularly in the vicinity of the vertical tail. The effect of the horizontal tail is expressed by the

term $K_{SH} \left[\frac{(A_{eV})_{H \text{ on}}}{(A_{eV})_{H \text{ off}}} - 1 \right]$ where $(A_{eV})_{H \text{ on}} / (A_{eV})_{H \text{ off}}$ may be obtained

from figure 18. The curves of figure 18 are presented for the specific

horizontal-tail size investigated (that is $\frac{S_H}{S_V} = 1.33$) and must be

corrected for any other size by the factor K_{SH} . If variations in size of the horizontal tail are assumed to have the same relative

effect on A_{eV} regardless of the horizontal-tail location, the factor K_{S_H} can be expressed as

$$K_{S_H} = \frac{\left[\frac{(A_{eV})_{H \text{ on}}}{(A_{eV})_{H \text{ off}}} \right]_{S_H/S_V} - 1}{\left[\frac{(A_{eV})_{H \text{ on}}}{(A_{eV})_{H \text{ off}}} \right]_{\frac{S_H}{S_V}=1.33} - 1}$$

This factor has been evaluated from the solid curve of figure 12(b) which represents the effects of variations in area of the horizontal tail, when located at the base of the vertical tail. Values of K_{S_H} , determined in this manner, are presented in figure 19.

The design procedure indicated by the use of figures 18 and 19 in conjunction with equation (1) can be expected to apply only at small angles of attack. At higher angles of attack, for the horizontal-tail locations below the midspan point on the vertical tail, the actual horizontal-tail contribution would be expected to be smaller than that predicted. For horizontal tails near the top of the vertical tail, the indicated procedure would be expected to lead to conservative results at higher angles of attack.

CONCLUSIONS

The results of an investigation to determine the effect of horizontal-tail size and position on the static-lateral-stability derivatives of a complete model with wing and tail surfaces having the quarter-chord line swept back 45° indicate the following conclusions:

1. Available procedures (based on analyses of unswept tail configurations) for predicting the contribution of a horizontal tail to

directional stability, have been found to be unreliable when applied to a tail configuration having 45° sweptback surfaces. The effects of variations in area and vertical location of the horizontal tail could be predicted qualitatively at zero angle of attack. The longitudinal location of the horizontal tail, except at the lower position, and the angle of attack were found to be important additional factors that could not be accounted for by available procedures.

2. For the wing-off configurations, increasing the area of the horizontal tail (when mounted at the base of the vertical tail) has a stabilizing effect at low angles of attack, but at high angles of attack the effect tended to become destabilizing.

3. The contribution of the horizontal tail to directional stability at zero angle of attack was beneficial when the horizontal tail was located at either the top or bottom of the vertical tail with the greatest benefit generally occurring for the top position. When located at the center of the vertical tail the effect of the horizontal tail generally was slightly adverse.

4. For the wing-off configurations, when the horizontal tail was mounted at the base of the vertical tail, the contribution of the horizontal tail to directional stability at small angles of attack became more favorable as it was moved toward the rear. At angles of attack near 20° , the contribution of the horizontal tail was unfavorable, regardless of its horizontal location.

5. For the wing-off configurations, when the horizontal tail was mounted near the top of the vertical tail, the contribution of the horizontal tail to directional stability at small angles of attack was favorable over the range of longitudinal locations investigated. At angles of attack near 20° , the largest favorable effect was obtained with the horizontal tail in the forward location.

6. The trends obtained with the wing on were similar to those obtained with the wing off, but a large decrease occurred in the favorable effect obtained at large angles of attack with the tail in the upper positions; a probable explanation was the detrimental effect of the wing wake arising from flow separation over the wing.

Langley Aeronautical Laboratory

National Advisory Committee for Aeronautics

Langley Air Force Base, Va., September 1, 1949

REFERENCES

1. Pass, H. R.: Analysis of Wind-Tunnel Data on Directional Stability and Control. NACA TN 775, 1940.
2. Murray, Harry E.: Wind-Tunnel Investigation of End-Plate Effects of Horizontal Tails on a Vertical Tail Compared With Available Theory. NACA TN 1050, 1946.
3. DeYoung, John: Theoretical Additional Span Loading Characteristics of Wings with Arbitrary Sweep, Aspect Ratio and Taper Ratio. NACA TN 1491, 1947.
4. Jacobs, Eastman N., and Ward, Kenneth E.: Interference of Wing and Fuselage from Tests of 209 Combinations in the N.A.C.A. Variable-Density Tunnel. NACA Rep. 540, 1935.
5. Goodman, Alex, and Fisher, Lewis R.: Investigation at Low Speeds of the Effect of Aspect Ratio and Sweep on Rolling Stability Derivatives of Untapered Wings. NACA TN 1835, 1949.
6. Goodman, Alex, and Brewer, Jack D.: Investigation at Low Speeds of Effect of Aspect Ratio and Sweep on Static and Yawing Stability Derivatives of Untapered Wings. NACA TN 1669, 1948.

TABLE I.— PERTINENT GEOMETRIC CHARACTERISTICS OF MODEL

Fuselage:

Length, inches	40.0
Fineness ratio	6.67

Wing:

Aspect ratio, A_W	4.0
Taper ratio, λ_W	0.6
Quarter-chord sweep angle, degrees	45
Dihedral angle, degrees	0
Twist, degrees	0
NACA airfoil section	65A008
Area, S_W , square inches	324
Span, b_W , inches	36
Mean aerodynamic chord, \bar{c}_W , inches	9.19

Vertical tail:

Aspect ratio, A_V	1.0
Taper ratio, λ_V	0.6
Quarter-chord sweep angle, degrees	45
NACA airfoil section	65A008
Area, S_V , square inches	48.6
Span, b_V , inches	6.97
Mean aerodynamic chord, c_V , inches	7.12
Tail length, l , inches	16.7
Area ratio, S_V/S_W	0.15
Tail-length ratio, l/b_W	0.464

Horizontal tail:

	H_1	H_2	H_3
Aspect ratio, A_H	4.0	4.0	4.0
Taper ratio, λ_H	0.6	0.6	0.6
Quarter-chord sweep angle, degrees	45	45	45
Dihedral angle, degrees	0	0	0
Twist, degrees	0	0	0
NACA airfoil section	65A008	65A008	65A008
Area, S_H , square inches	32.40	64.80	97.20
Span, b_H , inches	11.38	16.10	19.72
Mean aerodynamic chord, \bar{c}_H , inches	2.91	4.11	5.04
Area ratio, S_H/S_W	0.10	0.20	0.30
Area ratio, S_H/S_V	0.67	1.33	2.00

TABLE II.-- ORDINATES FOR NACA 65A008 AIRFOIL

[Station and ordinates in percent airfoil chord]

Station	Ordinate
0	0
.50	.62
.75	.75
1.25	.95
2.50	1.30
5.0	1.75
7.5	2.12
10.0	2.43
15	2.93
20	3.30
25	3.59
30	3.79
35	3.93
40	4
45	3.99
50	3.90
55	3.71
60	3.46
65	3.14
70	2.76
75	2.35
80	1.90
85	1.43
90	.96
95	.49
100	.02
L. E. radius: 0.408	



TABLE III.- CONFIGURATIONS INVESTIGATED

Wing off		Wing on	
Configuration (1)	Figure	Configuration (1)	Figure
F	9	W	9
F + V	15	W + F	9
		W + F + V	15
F + (H ₁) _{IM}	11(a)	-----	-----
F + (H ₂) _{IM}		-----	-----
F + (H ₃) _{IM}		-----	-----
F + V + (H ₁) _{IM}	11(b)	-----	-----
F + V + (H ₂) _{IM}		-----	-----
F + V + (H ₃) _{IM}		-----	-----
F + V + (H ₂) _{LF}	13(a)	W + F + V + (H ₂) _{LF}	14(a)
F + V + (H ₂) _{LM}		W + F + V + (H ₂) _{LM}	
F + V + (H ₂) _{LR}		W + F + V + (H ₂) _{LR}	
F + V + (H ₂) _{CF}	13(b)	W + F + V + (H ₂) _{CF}	14(b)
F + V + (H ₂) _{CM}		W + F + V + (H ₂) _{CM}	
F + V + (H ₂) _{CR}		W + F + V + (H ₂) _{CR}	
F + V + (H ₂) _{UF}	13(c)	W + F + V + (H ₂) _{UF}	14(c)
F + V + (H ₂) _{UM}		W + F + V + (H ₂) _{UM}	
F + V + (H ₂) _{UR}		W + F + V + (H ₂) _{UR}	

¹Notation:

W wing
 F fuselage
 V vertical tail

} For details, see figure 2.

H horizontal tail; subscripts 1, 2, and 3 refer to size (see fig. 3); letters L, C, and U refer to vertical location, and letters F, M, and R refer to horizontal location (see fig. 4).

NACA

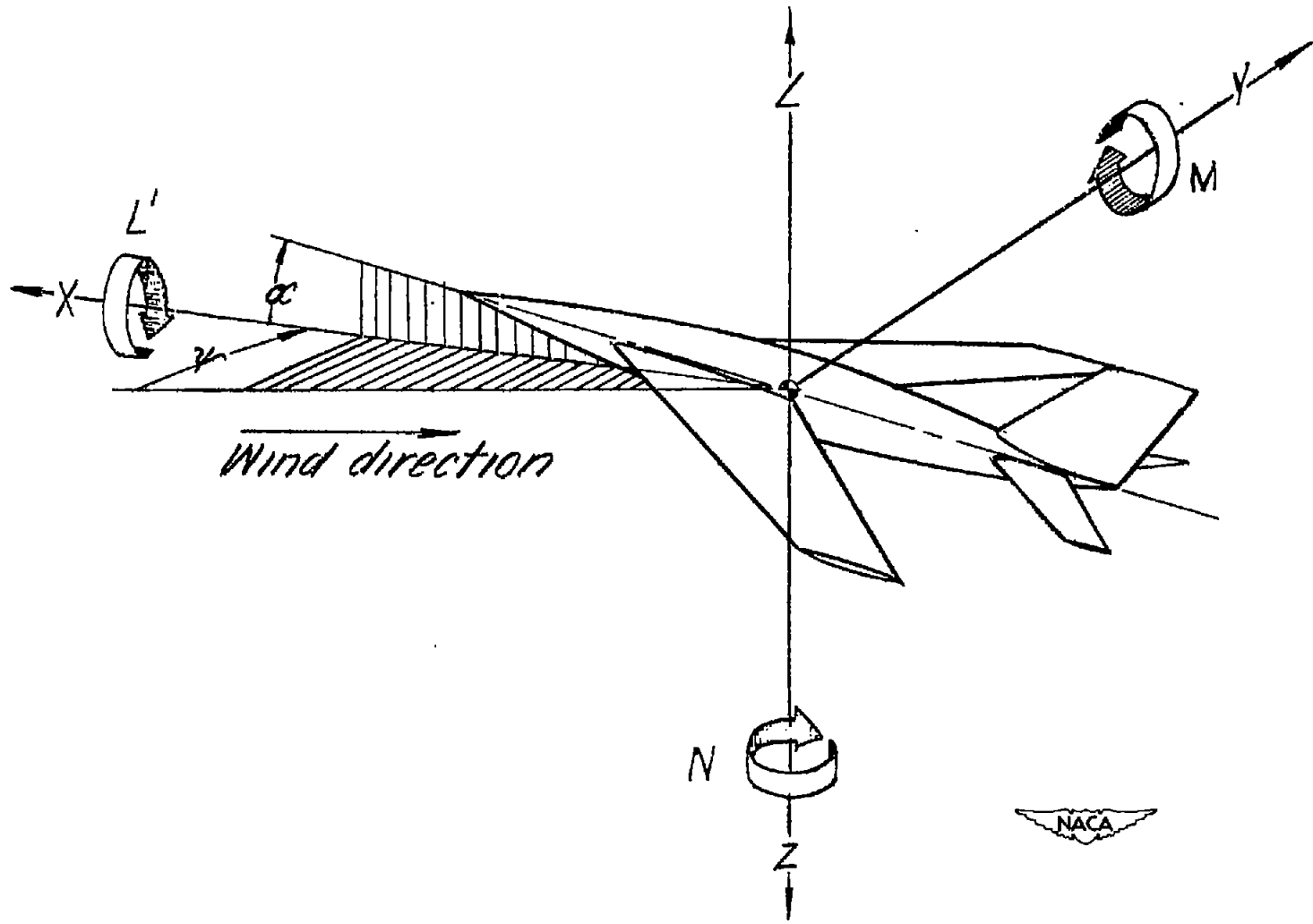


Figure 1.- System of axes used. Arrows indicate positive direction of angles, forces, and moments.

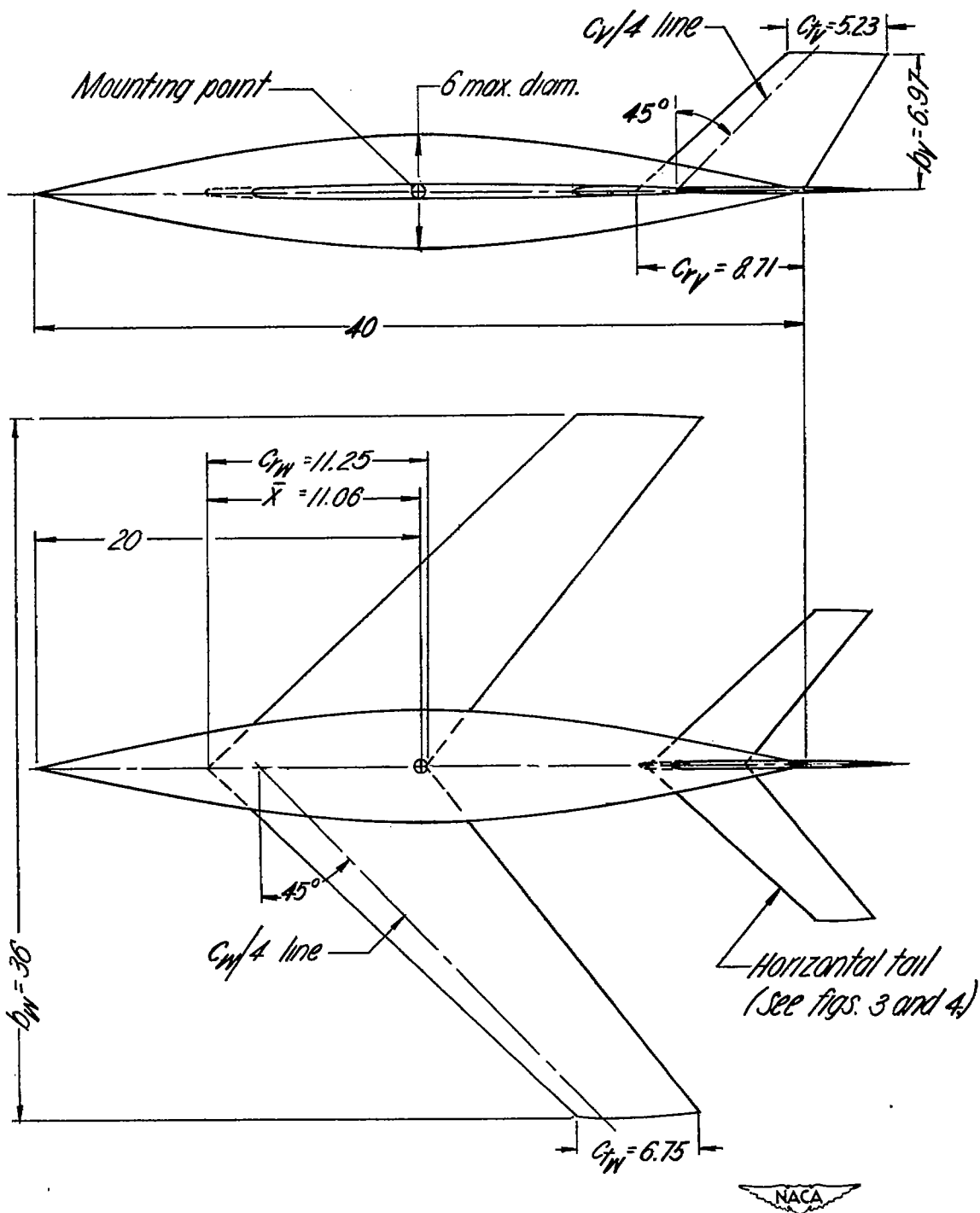


Figure 2.- Dimensions of the complete model. All dimensions are in inches.

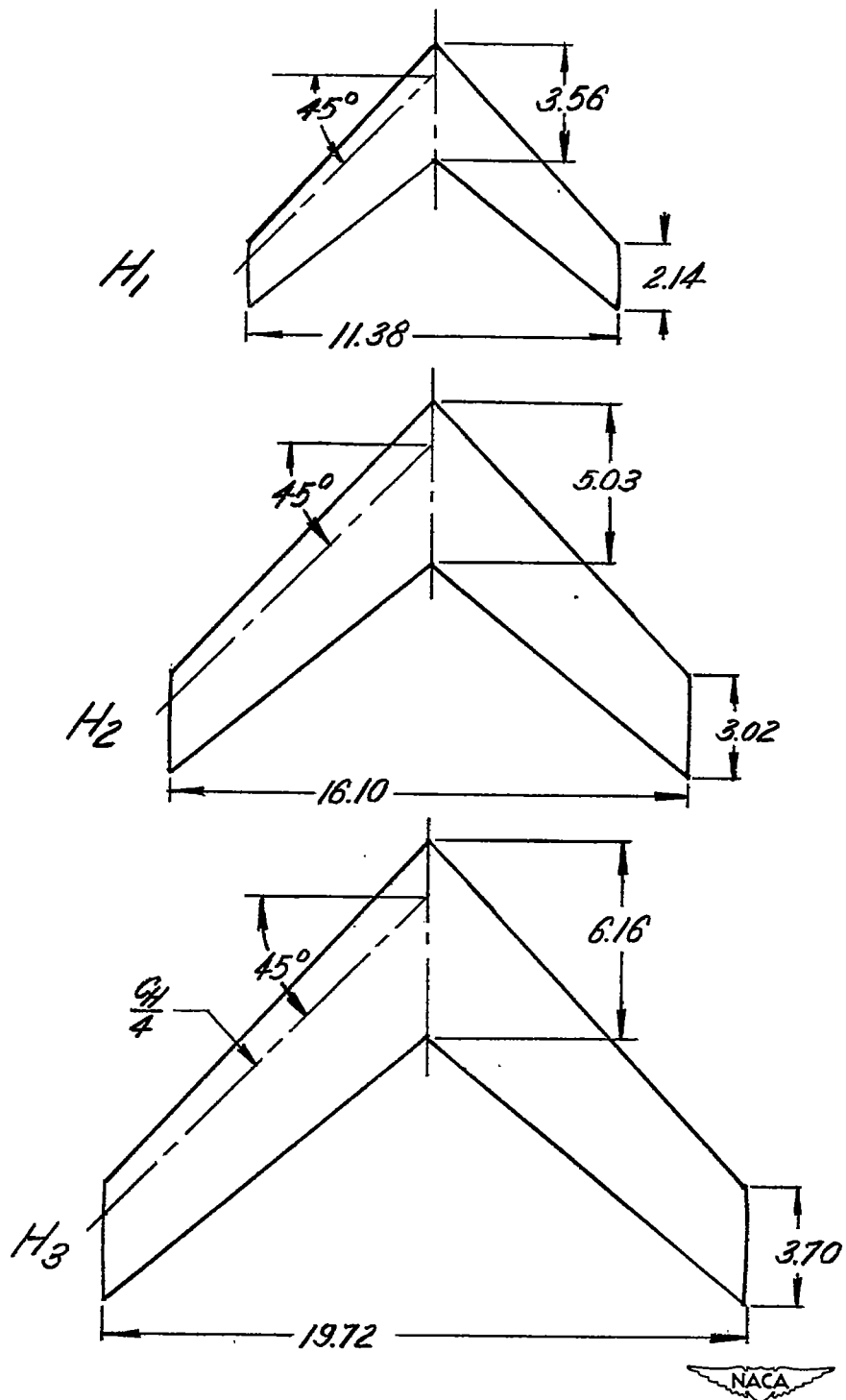


Figure 3.-Dimensions of the horizontal tails tested.
 Dimensions are in inches.

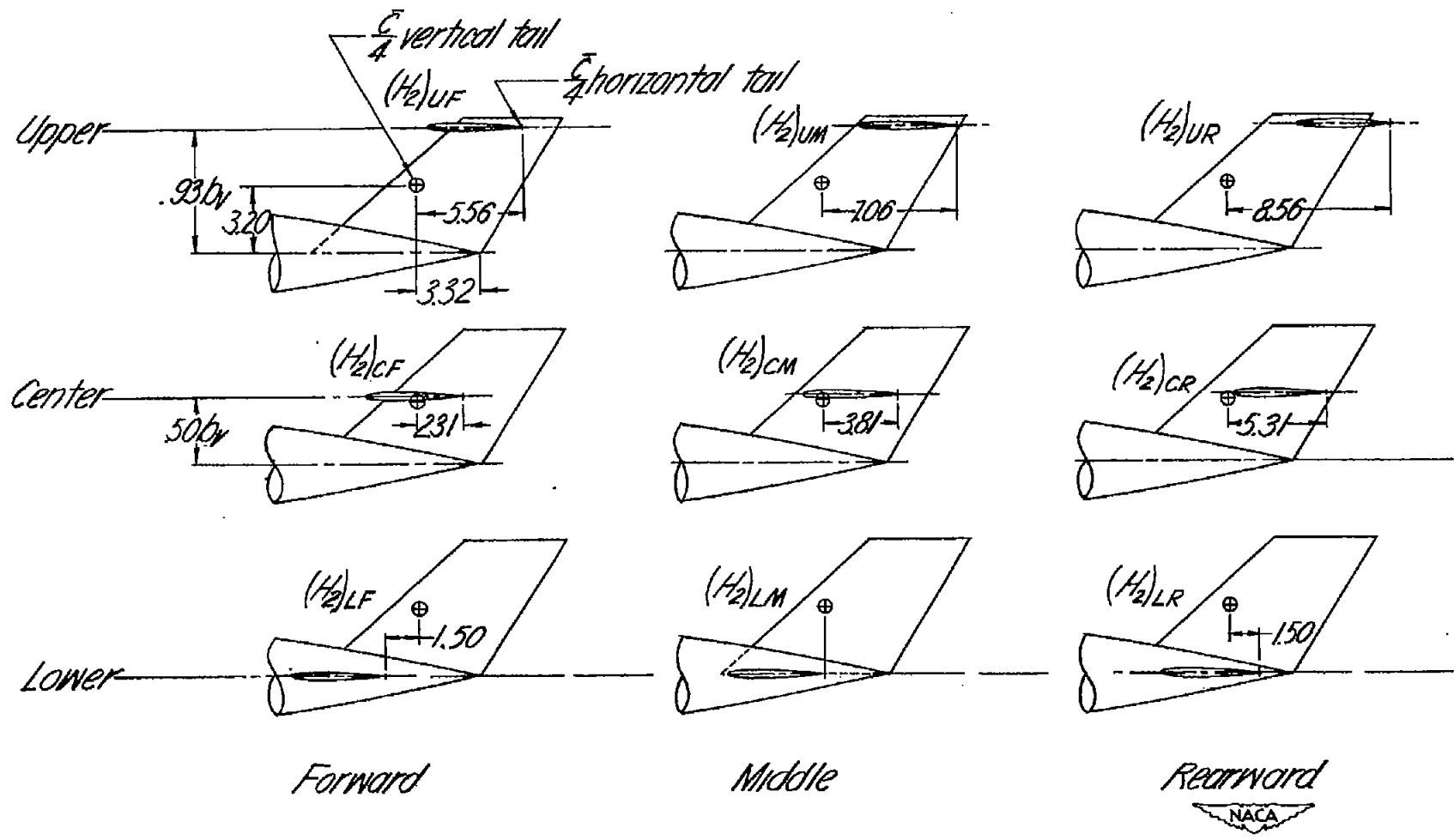


Figure 4.- Location of root chord of horizontal tail 2 when tested with vertical tail.
 Dimensions are in inches.

NACA TM 2010

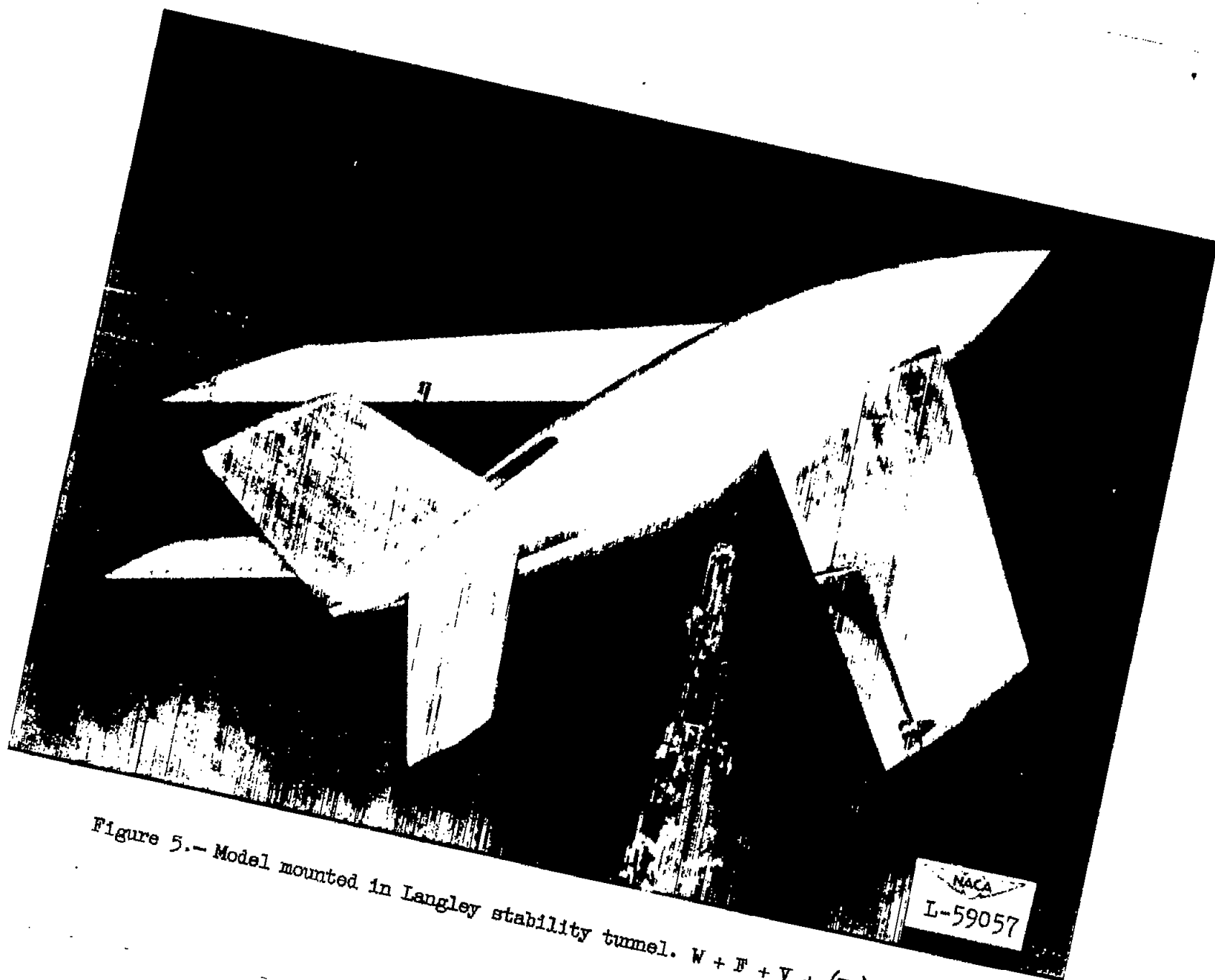


Figure 5.- Model mounted in Langley stability tunnel. $W + F + V + (H_2)_{IM}$



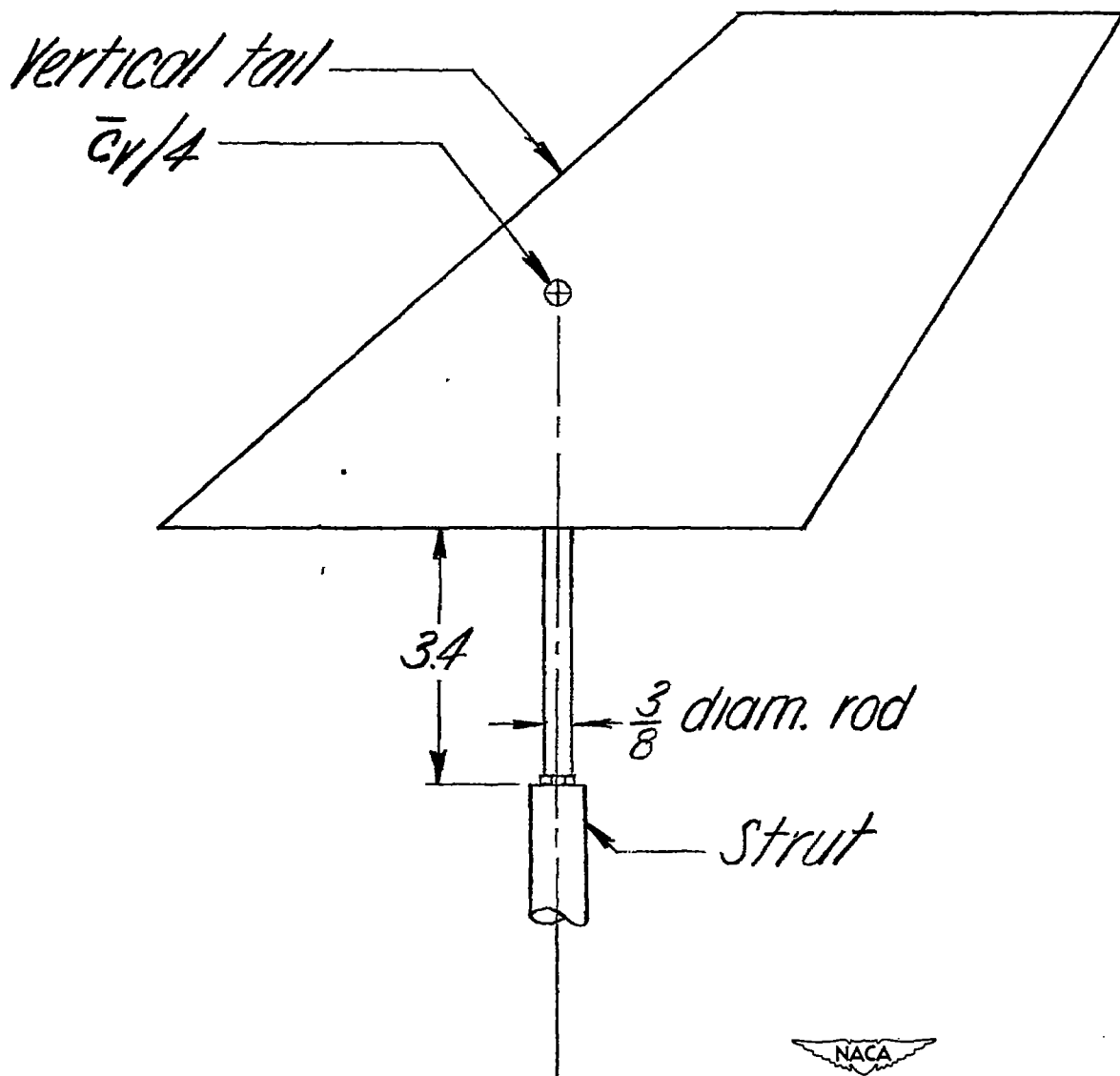


Figure 6.- Mounting arrangement for isolated vertical tail. Dimensions are in inches.

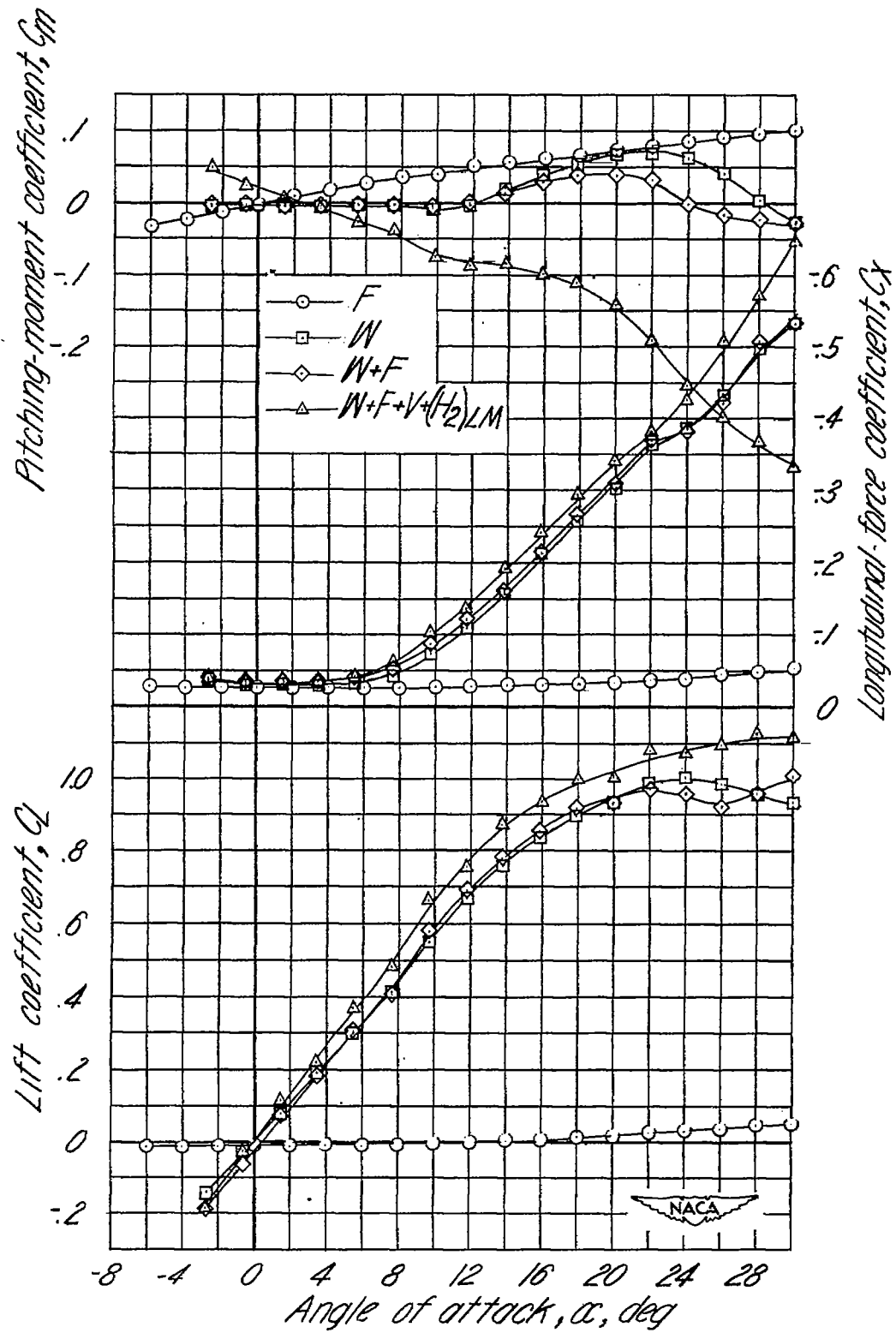


Figure 7.-Aerodynamic characteristics of some basic configurations.

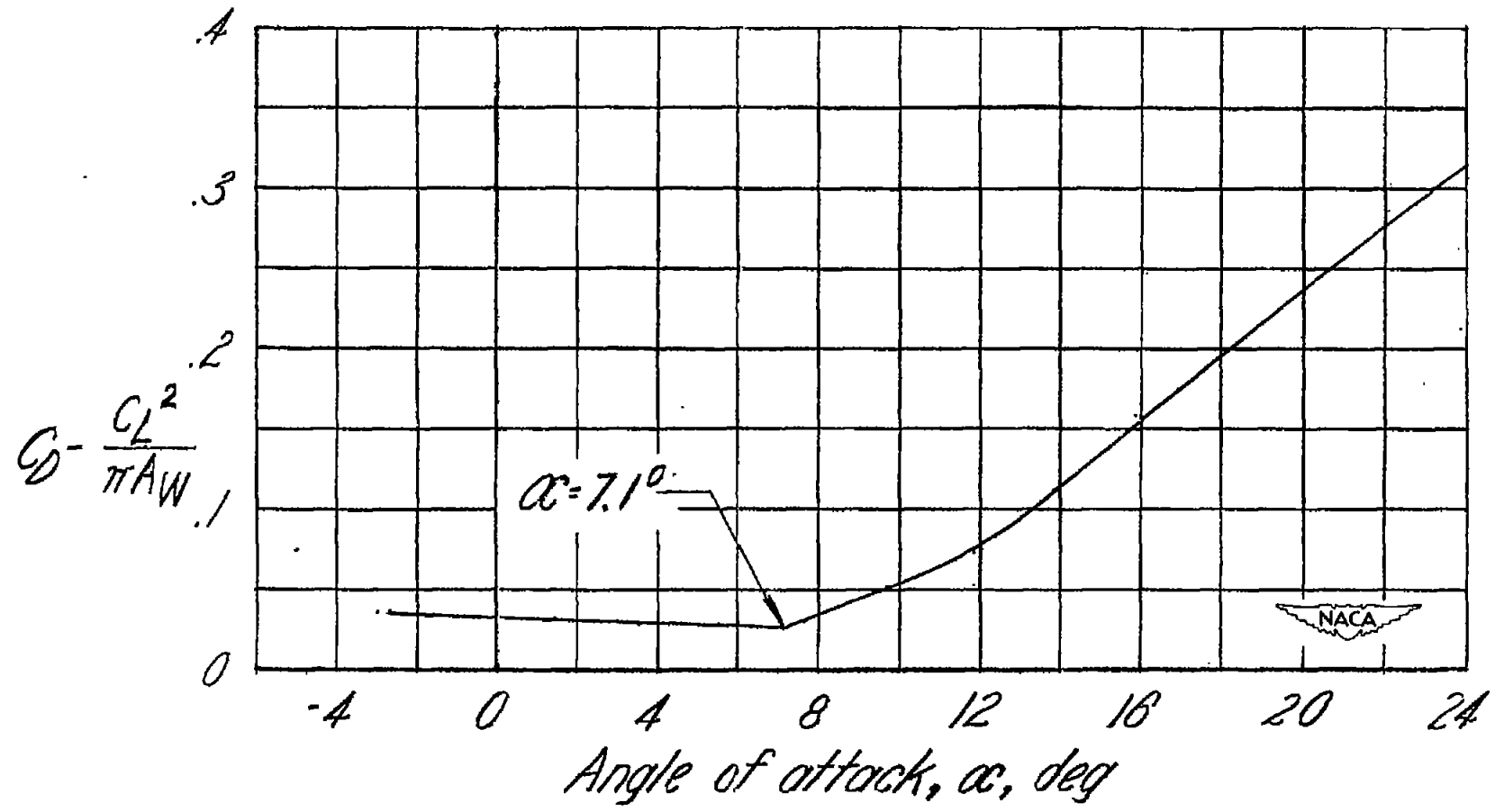


Figure 8.-Variation of $C_D - \frac{C_L^2}{\pi A_W}$ with α . Wing alone.

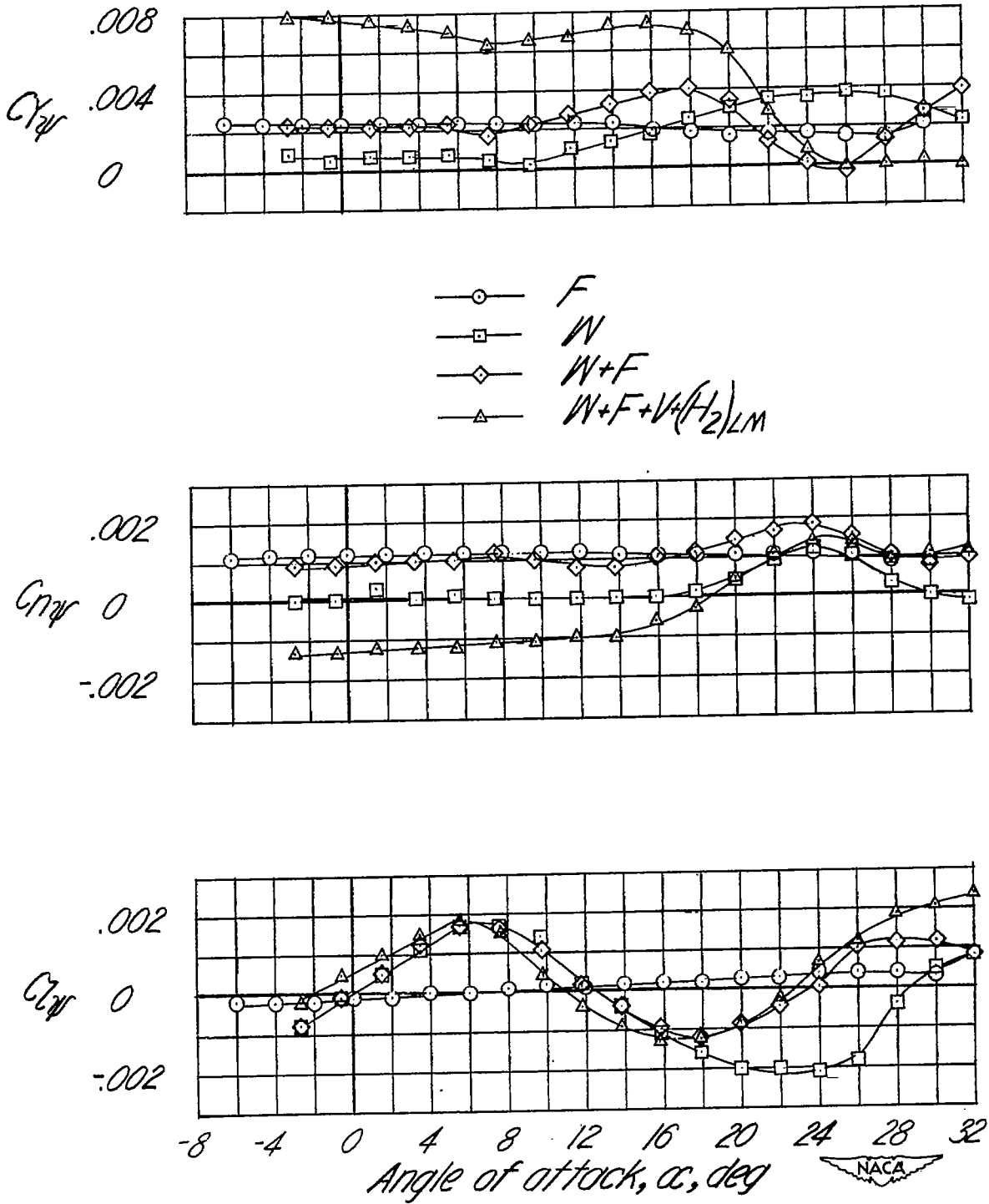


Figure 9.-Variation of C_{YR} , C_{NR} , and C_{LR} with angle of attack for some basic configurations.

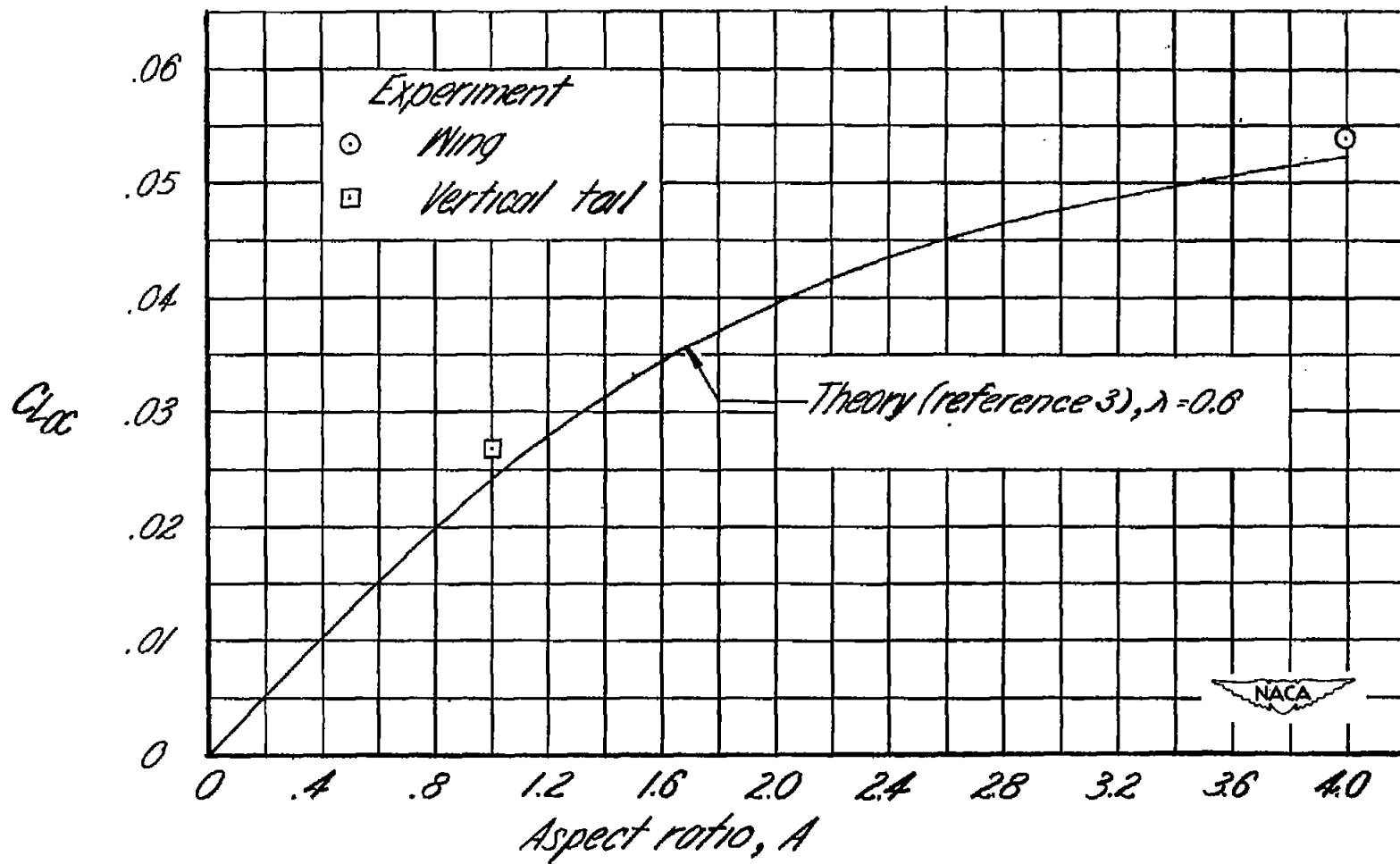
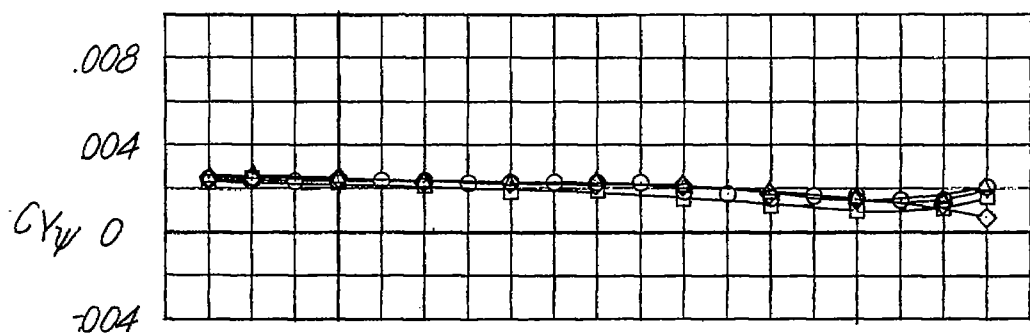
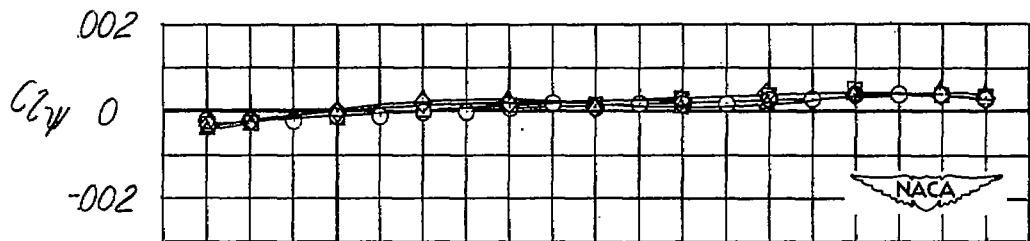
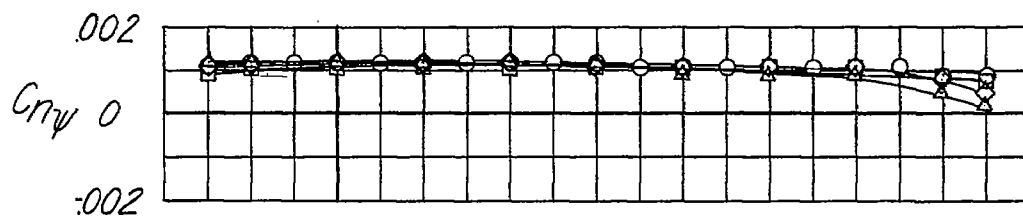


Figure 10.- Comparison with theory of experimental lift-curve slopes. Wing and vertical tail; $\alpha = 0^\circ$.



Configuration

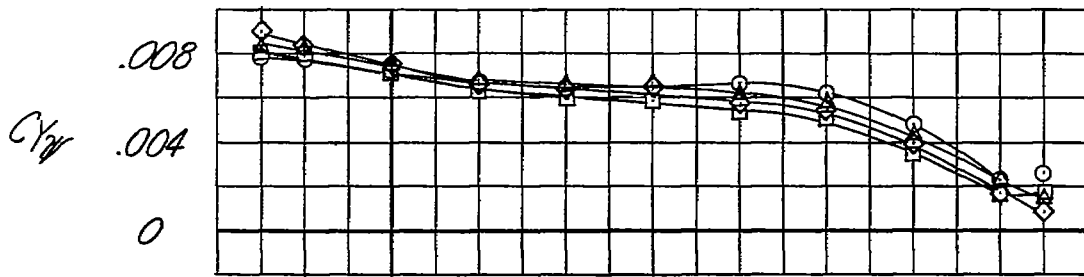
- F
- $F+(H_1)_{LM}$
- ◇ $F+(H_2)_{LM}$
- △ $F+(H_3)_{LM}$



-8 -4 0 4 8 12 16 20 24 28 32
Angle of attack, α , deg

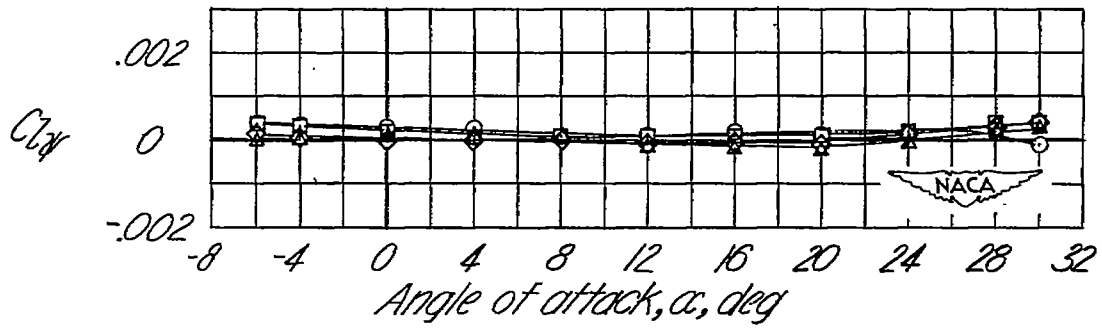
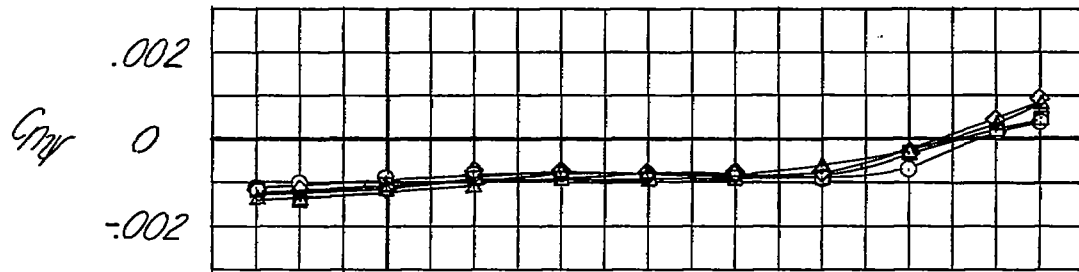
(a) Vertical tail off.

Figure 11.-Effect of change in horizontal tail area on C_{Yw} , C_{mw} , and C_{zeta} . Wing off.



Configuration

- $F+V$
- $F+V+(H_1)_{LM}$
- ◇— $F+V+(H_2)_{LM}$
- △— $F+V+(H_3)_{LM}$



(b) Vertical tail on.
Figure 11.-Concluded.

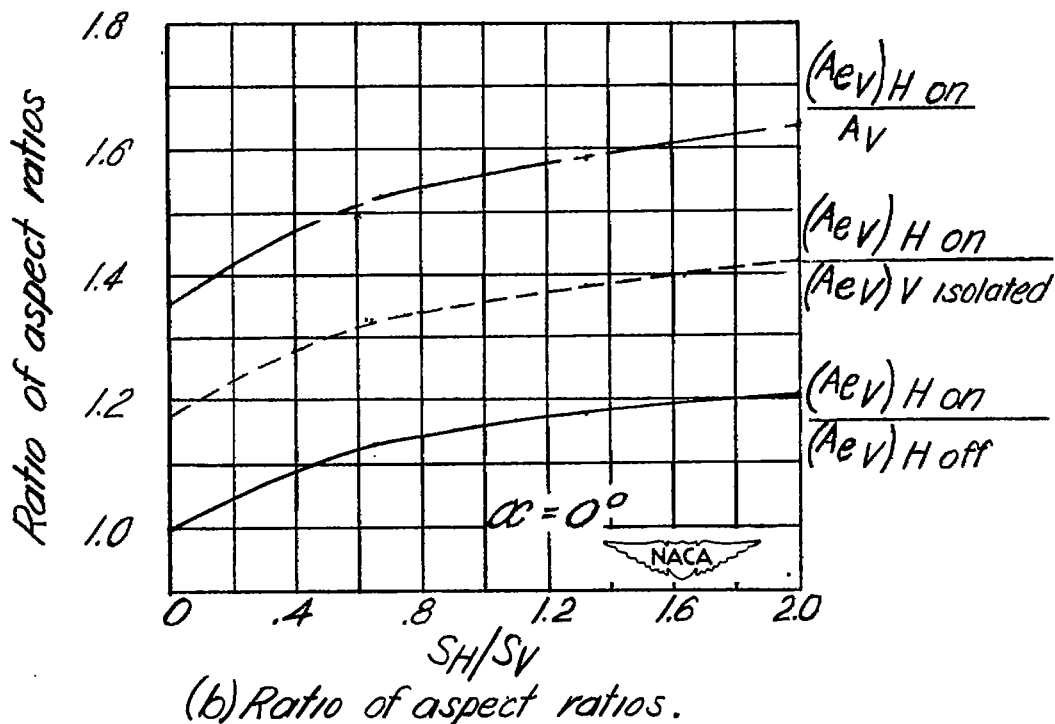
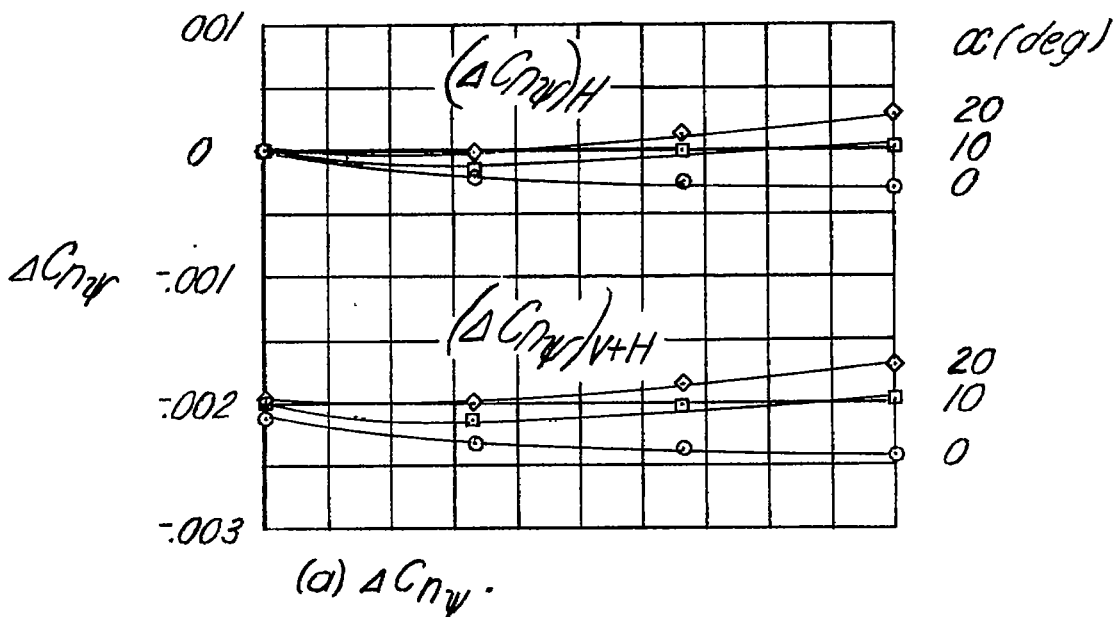
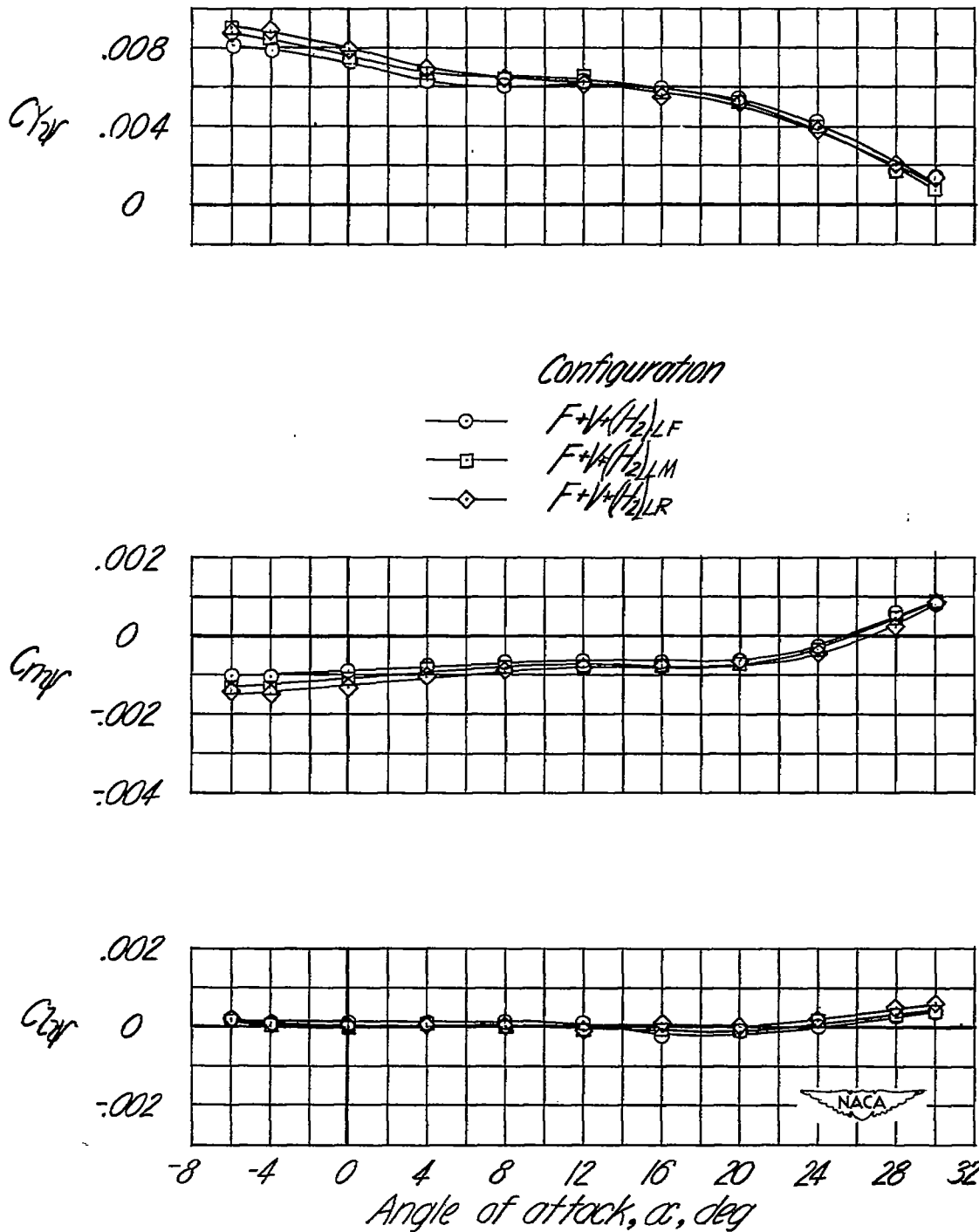
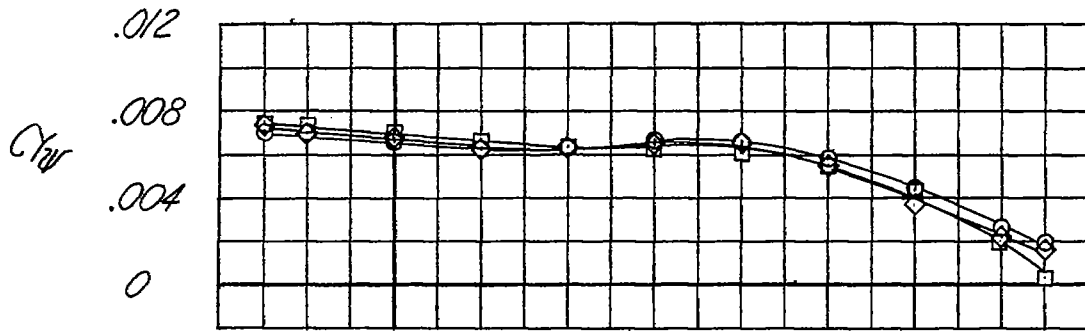


Figure 12. -Effect of horizontal-tail area on the contribution of the vertical tail to directional stability and on the effective aspect ratio of the vertical tail. Location of horizontal tail, LM. Wing off.



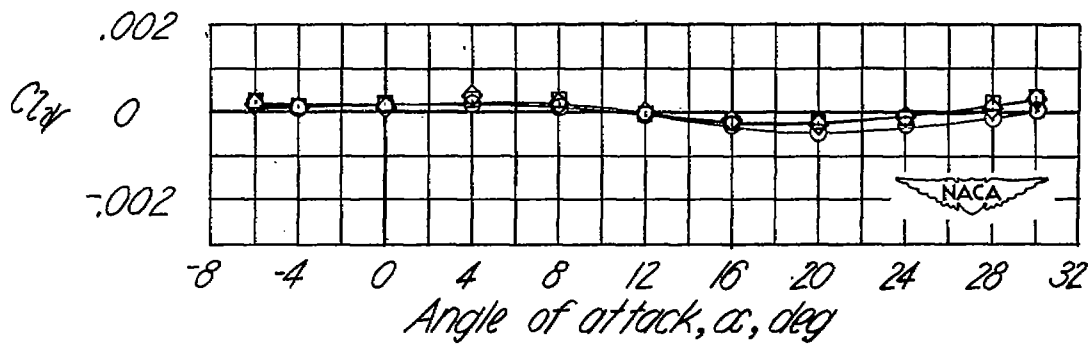
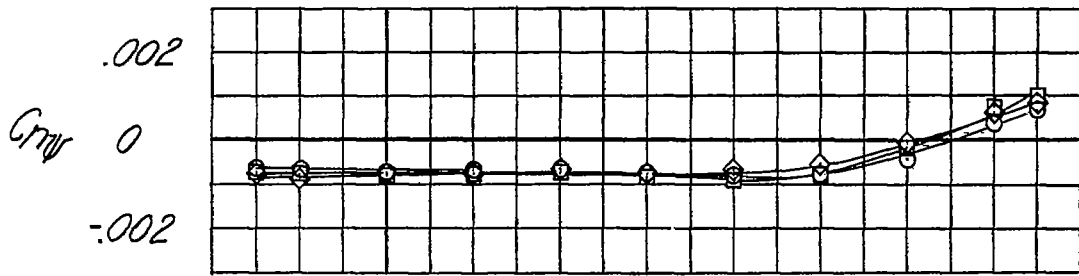
(a) Lower position.

Figure 13.-Effect of horizontal displacement of the horizontal tail on C_{Yr} , C_{Nr} , and C_{Lr} . Wing off.



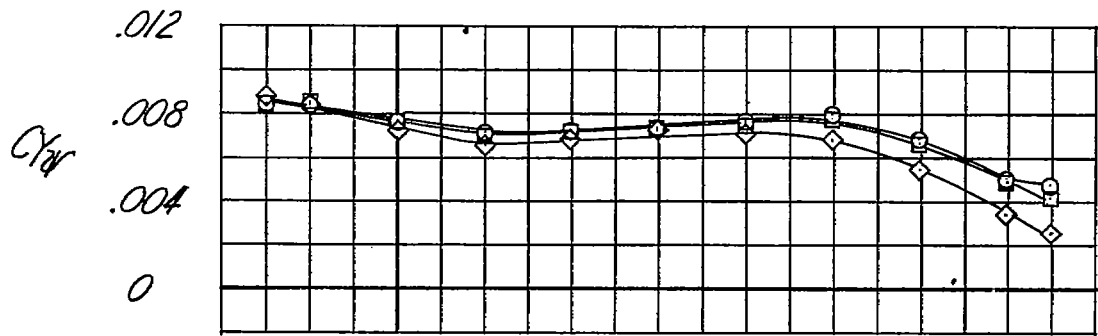
Configuration

- $F + \sqrt{A} (1/2)_{CF}$
- $F + \sqrt{A} (1/2)_{CM}$
- ◇— $F + \sqrt{A} (1/2)_{CR}$



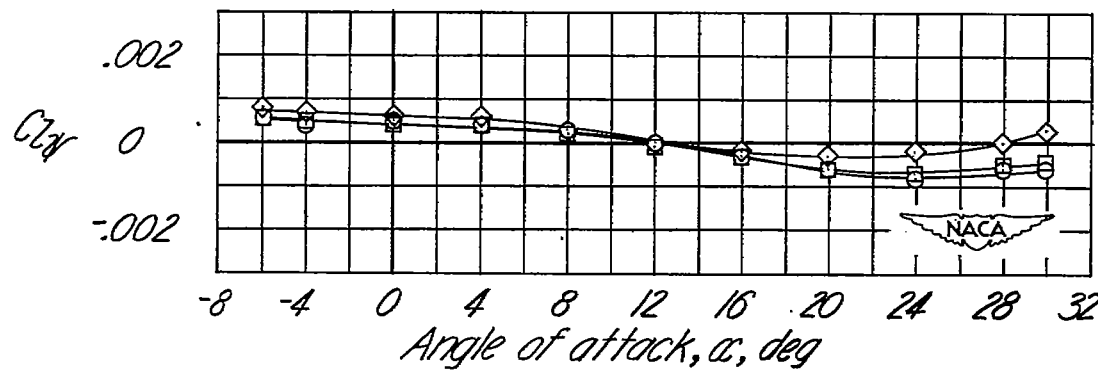
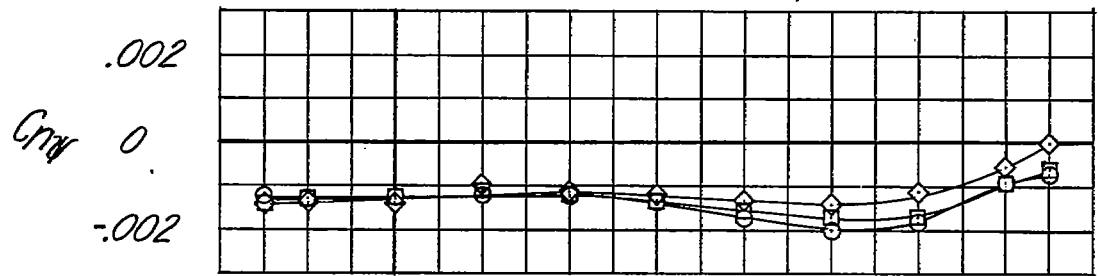
(b) Center position.

Figure 13.-Continued.



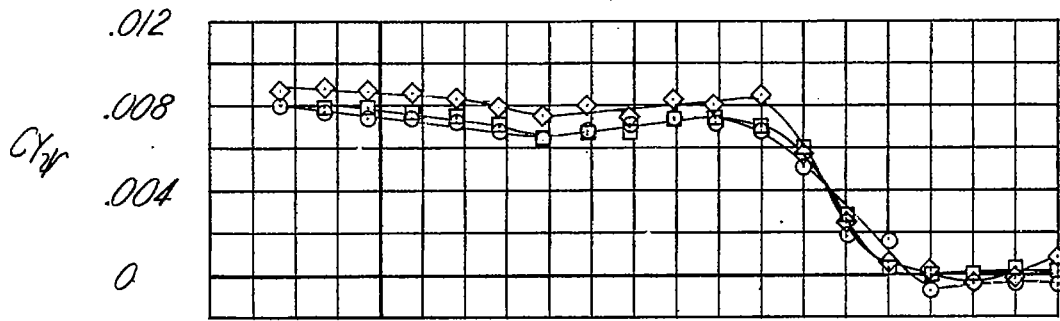
Configuration

- $F+V+(1/2)_{UF}$
- $F+V+(1/2)_{UM}$
- ◇ $F+V+(1/2)_{UR}$



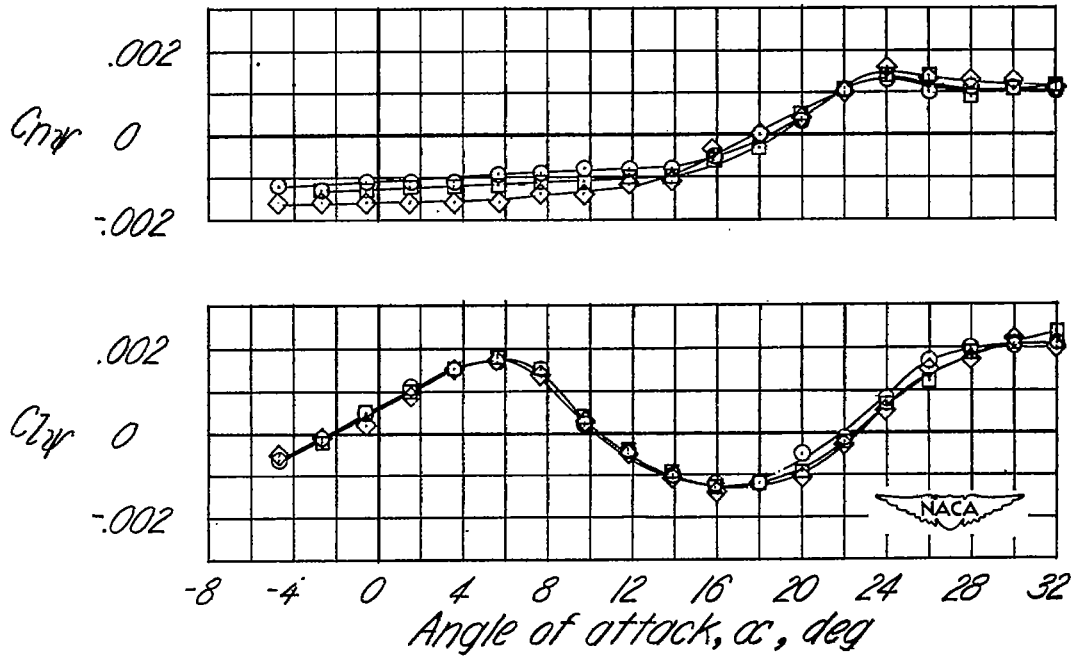
(c) Upper position.

Figure 13-Concluded.



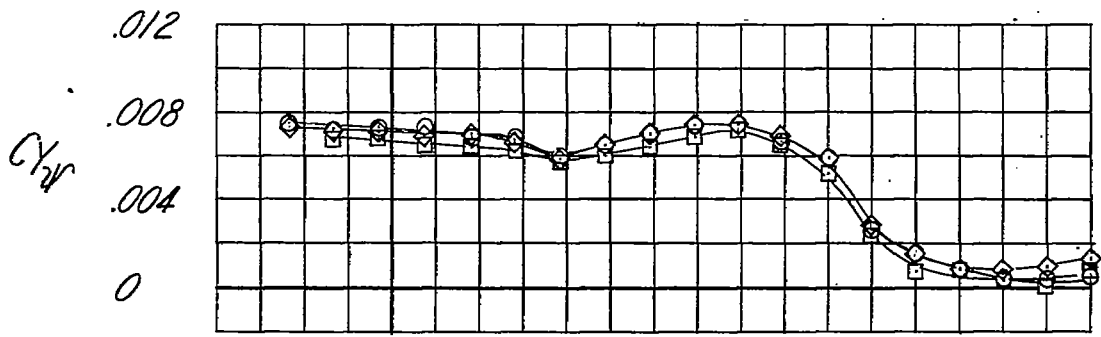
Configuration

- — $W+F+V+(1/2)_{LF}$
- — $W+F+V+(1/2)_{LM}$
- ◇ — $W+F+V+(1/2)_{LR}$



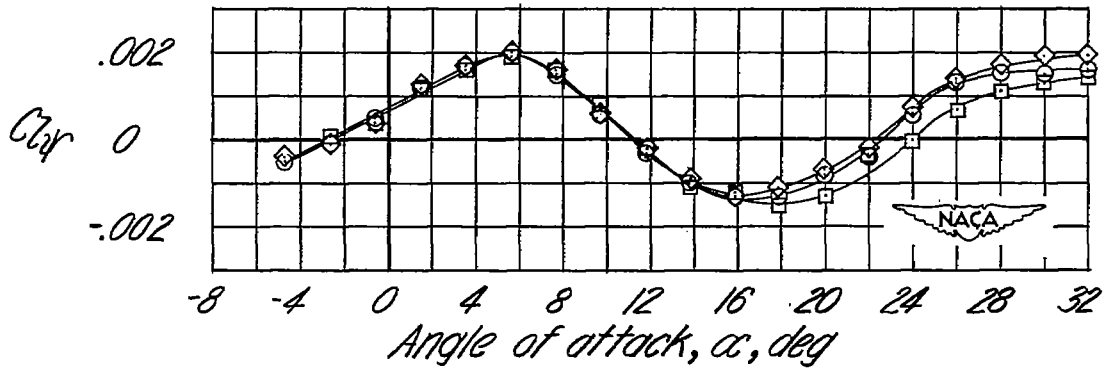
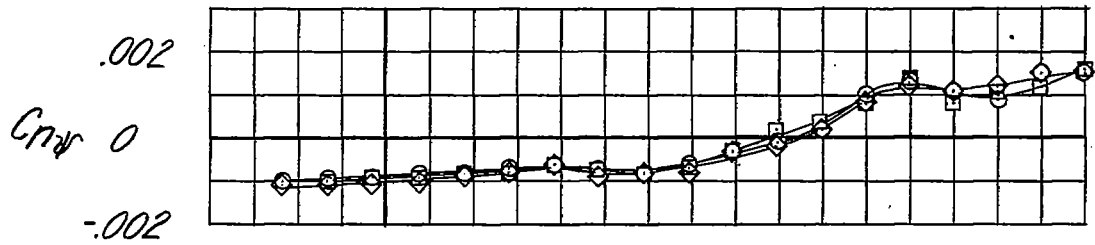
(a) Lower position.

Figure 14.-Effect of horizontal displacement of the horizontal tail on C_{Yr} , C_{mr} , and C_{Lr} . Wing on.

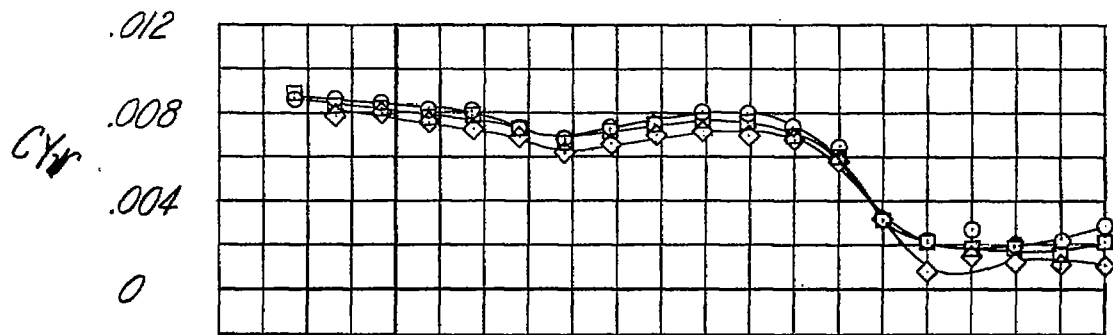


Configuration

- $W+F+V+(\frac{1}{2})_{CF}$
- $W+F+V+(\frac{1}{2})_{CM}$
- ◇— $W+F+V+(\frac{1}{2})_{CR}$

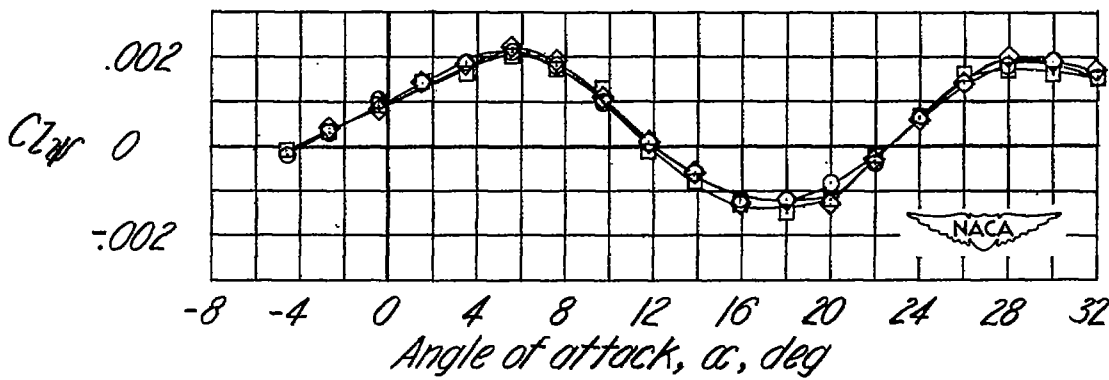
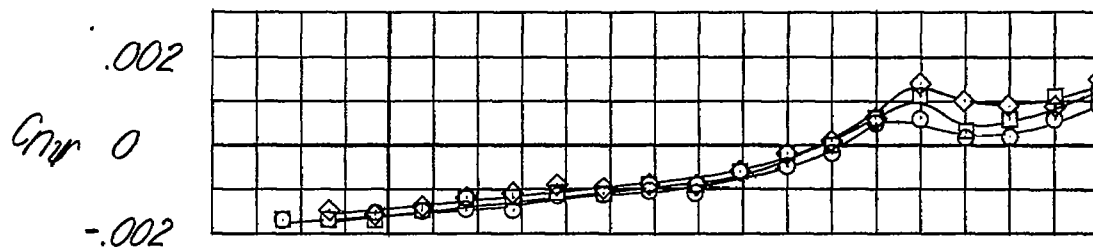


(b) Center position.
Figure 14.-Continued.



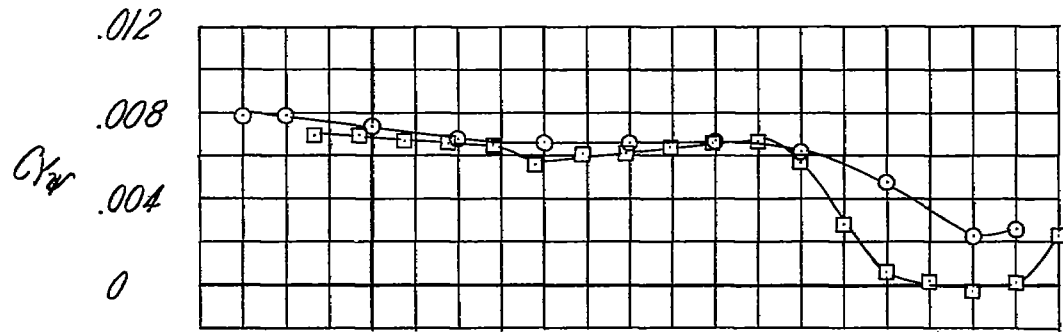
Configuration

- $W+F+V+(H_2)_{UF}$
- $W+F+V+(H_2)_{UM}$
- ◇— $W+F+V+(H_2)_{UR}$



(c) Upper position.

Figure 14.- Concluded.



Configuration
 —○— F+V
 —□— W+F+V

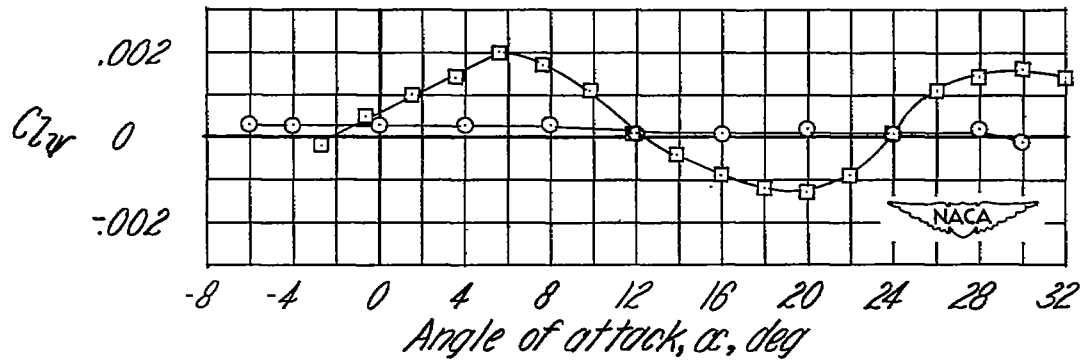
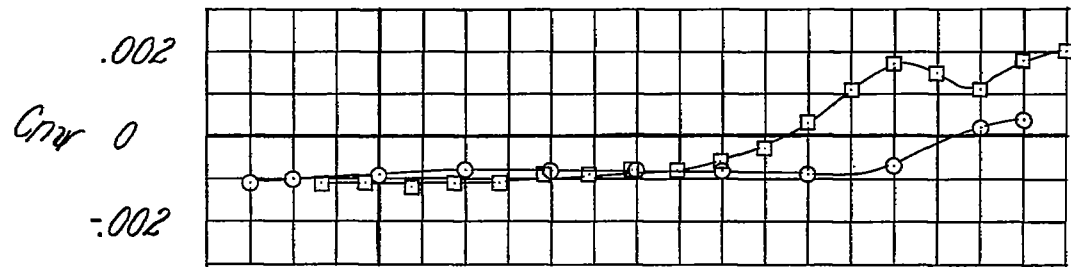


Figure 15-Effect of adding wing on C_{yw} , C_{nw} , and C_{zw} . Vertical tail on; horizontal tail off.

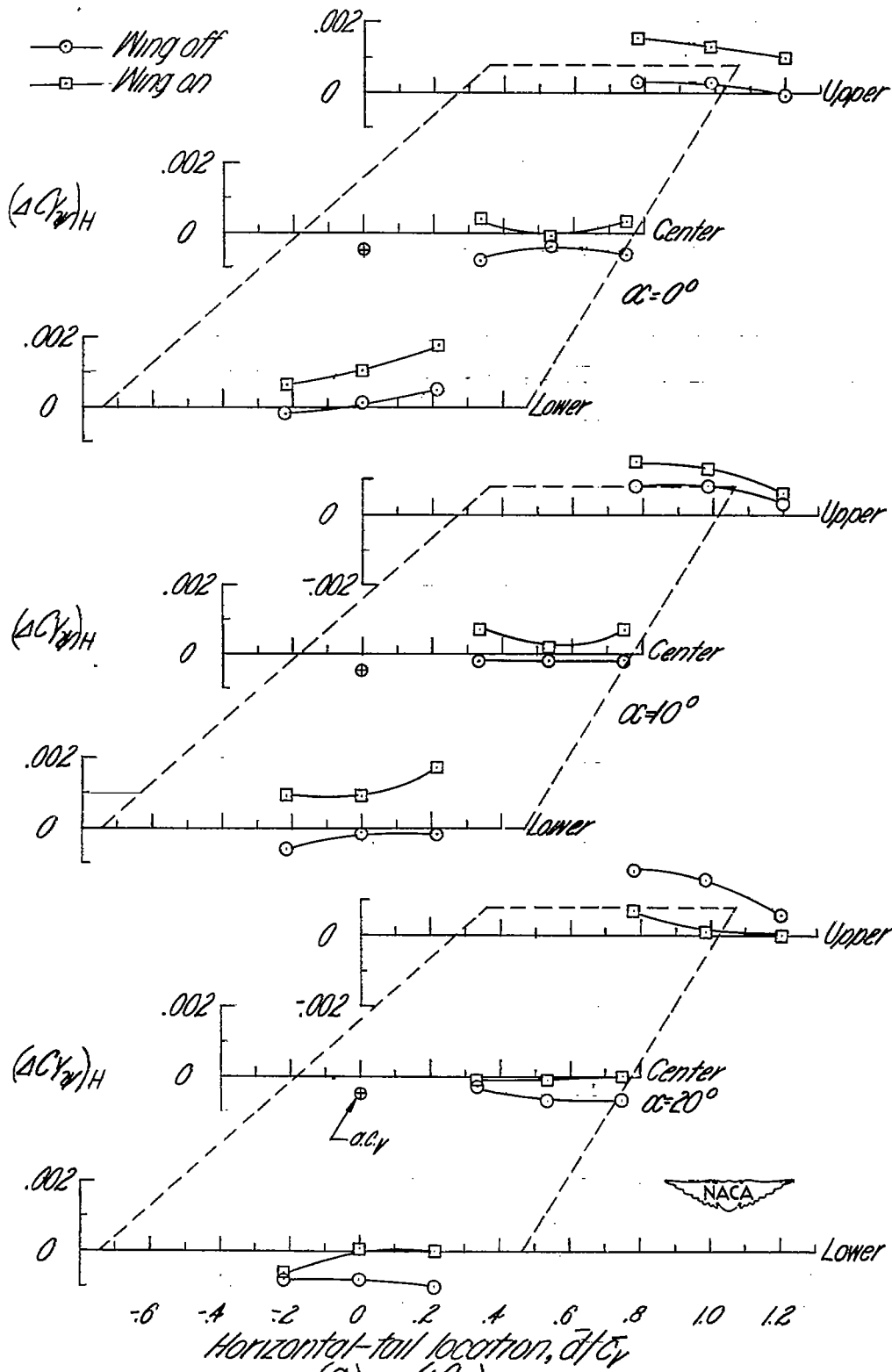
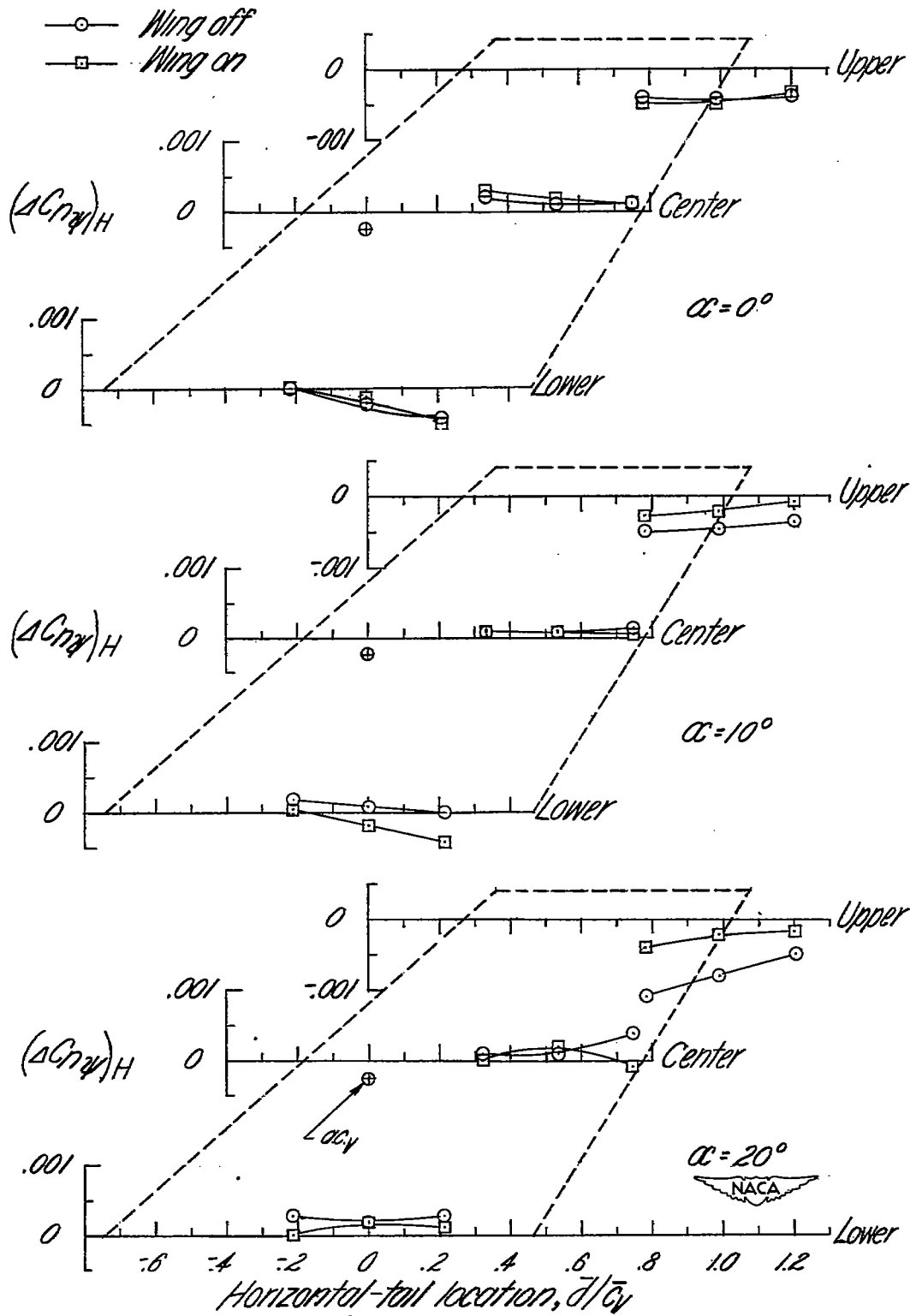
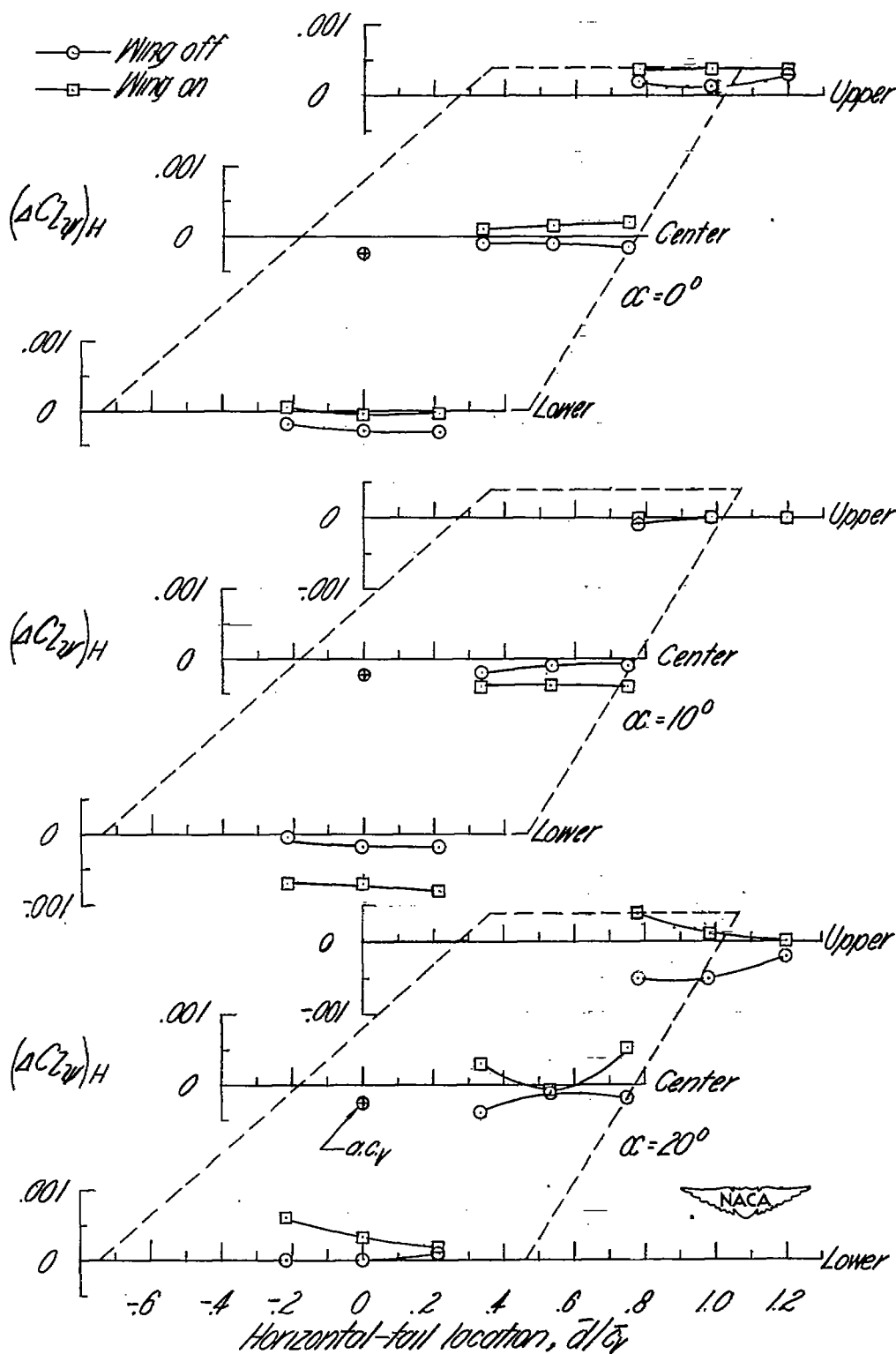


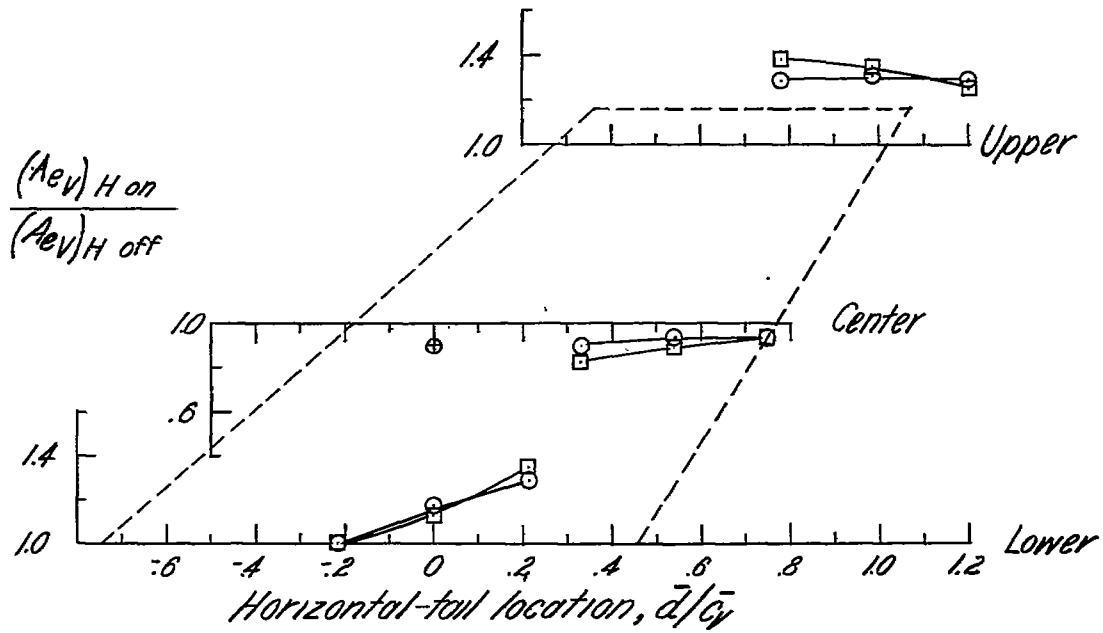
Figure 16.-Increment in C_{LH} , C_{TH} , and C_{DH} effected by horizontal tail 2.



(b) $(\Delta C_{LH})_H$.
 Figure 16.-Continued.

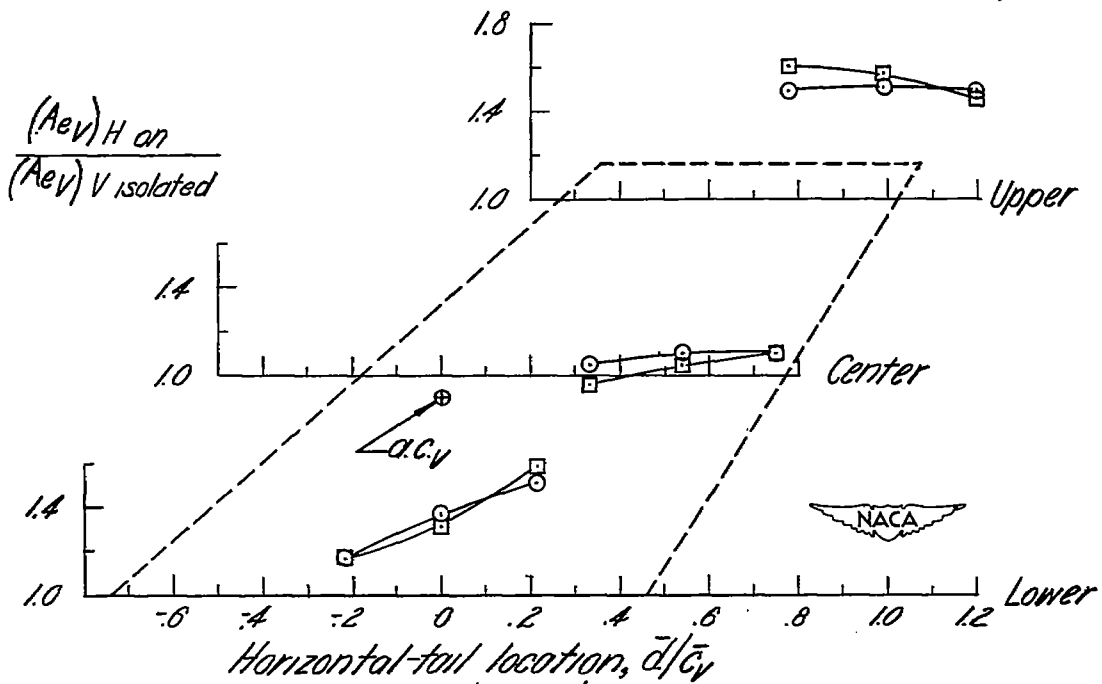


(c) $(\Delta C_{l_w})_H$.
 Figure 16.-Concluded.



(a) $(AeV)_{H \text{ on}} / (AeV)_{H \text{ off}}$.

○ Wing off
 □ Wing on



(b) $(AeV)_{H \text{ on}} / (AeV)_{V \text{ isolated}}$.

Figure 17.- Change in effective aspect ratio of vertical tail caused by horizontal tail 2. $\alpha = 0^\circ$.

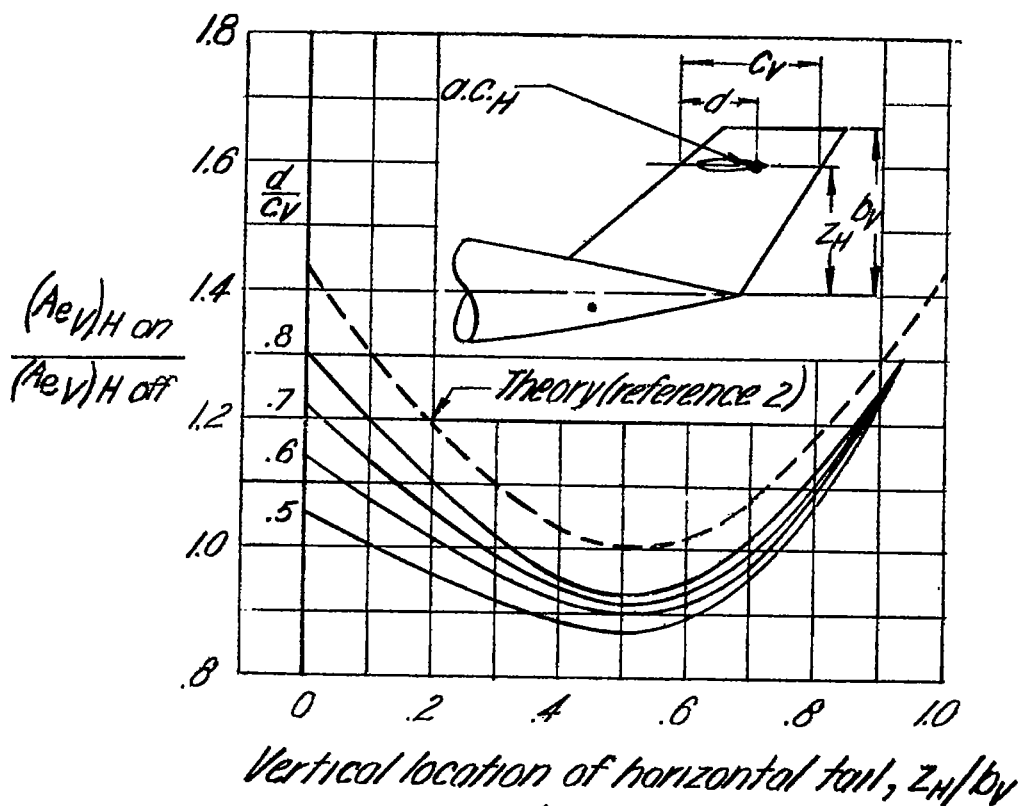


Figure 18.-Variation of $\frac{(AeV)H_{on}}{(AeV)H_{off}}$ with horizontal-tail position. $\alpha = 0^\circ$; wing off.

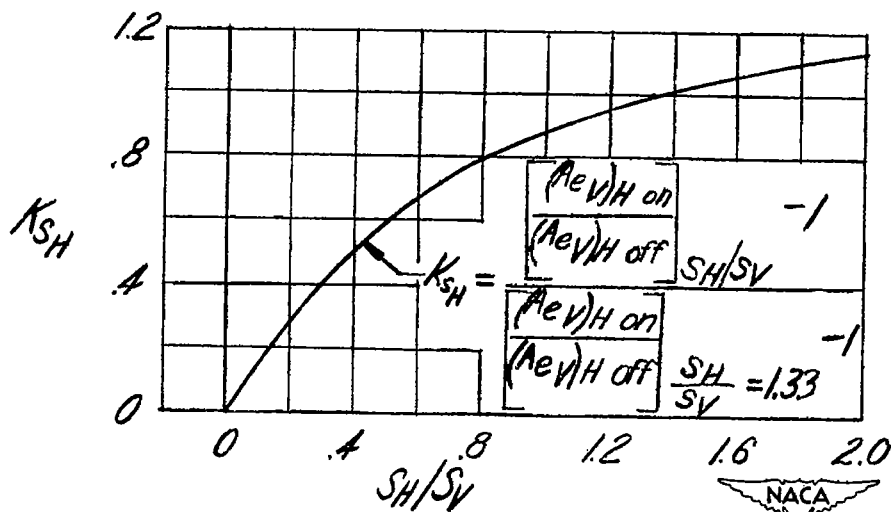


Figure 19.-Variation of K_{SH} with horizontal-tail area.